Monthly Notices
of the
ROYAL ASTRONOMICAL SOCIETY

MNRAS **509,** 4229–4245 (2022)
Advance Access publication 2021 September 16

https://doi.org/10.1093/mnras/stab2633

# 20 Orbits of binaries based on soar speckle observations

Jorge Gómez,[1,2] José A. Docobo,[1,2,3]★ Pedro P. Campo,[1,2]★ Manuel Andrade,[1,2,4] Rene A. Mendez.[5]★ and Edgardo Costa[5]

[1]*Observatorio Astronómico Ramón María Aller, Universidade de Santiago de Compostela (USC), Avenida das Ciencias s/n, Campus Vida, Santiago de Compostela, E-15782 Galiza, Spain*
[2]*Instituto de Matemáticas and Departamento de Matemática Aplicada, Facultade de Matemáticas, USC, Rúa Lope Gómez de Marzoa, s/n, Campus Vida, Santiago de Compostela, E-15782 Galiza, Spain*
[3]*Real Academia de Ciencias de Zaragoza, Facultad de Ciencias, C/ Pedro Cerbuna 12, E-50009 Zaragoza, Spain*
[4]*Escola Politécnica Superior de Enxeñaría, USC, Benigno Ledo s/n, Campus Terra, Lugo, E-27002 Galiza, Spain*
[5]*Universidad de Chile, Casilla 36-D, Santiago, Chile*

Accepted 2021 September 9. Received 2021 August 30; in original form 2021 June 3

## ABSTRACT

New observational data obtained during the 2018, 2019, and 2020 speckle runs with the 4.1-m Southern Astrophysical Research (SOAR) telescope located at Cerro Pachón (Chile) allowed us to recalculate the orbits of the visual binaries: WDS 00277-1625 (YR 1 Aa,Ab), WDS 00462-2214 (RST4155), WDS 03124-4425 (JC 8), WDS 07427-3510 (HDS 1091), WDS 10093+2020 (A2145), WDS 10116+1321 (HU 874 AB), WDS 10217-0946 (BU 25), WDS 11585-2350 (RST 3767 AB), WDS 13117-2633 (FIN 305), WDS 13305+0729 (A 1789), and WDS 16458-0046 (A1141). In addition, we present the first orbits calculated for the following binaries: WDS 07303-5657 (FIN 105), WDS 09110-1929 (I 824), WDS 12111-5302 (HU 1604), WDS 14592-4206 (HDS 2116 Aa,Ab), WDS 15157-2736 (BU 350), WDS 15493+0503 (A 1126), WDS 16402-2800 (VOU 44 AB), and WDS 18126+1224 (HDS 2570). All of them are placed below Dec. + 21° and the majority are main-sequence stars. Except in cases with giant components or close triple systems, the ANAPAR method was used in order to obtain precise dynamical parallaxes and individual masses. These parallaxes were compared with those obtained by *Gaia* and/or *Hipparcos* satellites. In the case of FIN 305, we present two different orbital solutions. Also, using the dynamical parallaxes given by these orbits, we have been able to calculate the luminosity of these systems. Said luminosities allow us to indicate an approximate age for the components of these systems, situating them within the Hertzsprung-Russell (HR) diagram. In addition, a commentary for each binary about the physical and dynamical properties of the studied binaries has been included.

**Key words:** techniques: high angular resolution – astrometry – binaries: visual – stars: fundamental parameters.

## 1 INTRODUCTION

Speckle interferometry was discovered and first applied 50 yr ago (Labeyrie 1970), and it continues to yield astrometric and photometric data that are especially important for the study of binary and multiple star systems. The determination of close visual orbits combined with the parallaxes measured by *Gaia* (Gaia Collaboration 2016, 2018) allows us to calculate the total mass of the system and estimate approximate values for the masses of each component based on the difference of magnitude between the components and their spectral decomposition. Moreover, using the ANAPAR method (Andrade 2019), we cannot only obtain very precise values of the dynamical parallaxes but also the individual masses, except in cases when there is a giant component in a system. In this article, we have used measurements of the Southern Astrophysical Research (SOAR) 2018 (Tokovinin et al. 2019), 2019, and 2020 speckle runs in order to calculate new orbits for 11 systems that need to be improved. The orbits as well as their corresponding physical parameters of another eight systems: FIN 105, I 824, HU 1604, HDS 2116 Aa,Ab, BU 350, A 1126, VOU 44 AB, and HDS 2570 were calculated for the first time. Except in the cases with giant components, the *Gaia* and the *Hipparcos* parallaxes have been compared with the dynamical parallaxes.

The HRCam, a fast imager that works either as a standalone instrument or with SOAR Adaptive Module (SAM; Tokovinin et al. 2016) was used in all of those observational speckle runs.

The device is installed at the 4.1-m SOAR telescope located at Cerro Pachón (Chile) and allows for interferometry combined with adaptive optics yielding resolutions in the 0.012–3.37 arcsec range. In a typical observing run, the calibration measurements are characterized by rms errors of 0°1–0°2 in orientation and 0.002–0.004 in scale. SOAR speckle runs were specifically designed to collect a large quantity of relevant data from well known, less known, and even from those systems with undetected subcomponents (Tokovinin 2018a). The SOAR speckle campaigns (Tokovinin et al. 2015, 2018, 2019; Tokovinin 2016) increase the number of measurements and

★ E-mail: joseangel.docobo@usc.es (JAD); pedropablo.campo@usc.es (PPC); rmendez@uchile.cl (RAM)

the quality of the samples of the orbits of southern systems year by year. As a matter of fact, these data were used in several orbital calculations (e.g. Tokovinin 2017, 2018b; Mendez et al. 2017; Mason et al. 2018) and consequently, in the precise determination of stellar masses and dynamical parallaxes.

Together with the precise data provided by SOAR, the whole set of previous measurements, those available in the USNO Catalogue of Interferometric Measurements of Binary Stars (Hartkopf, McAlister & Mason 2001b) and also those included in the historical data base of micrometric measurements, (Worley & Douglass 1997), have been used. The weights of the visual observations follow the scheme shown in Docobo & Ling (2003), whereas for the interferometric measurements we have assigned them according to the aperture of the telescope: weight 5 for apertures smaller than 1, 10 for 1-2, 15 for 2-4, 20 for 4-6 m., and 30 for larger apertures. To improve or calculate from the beginning all of those orbits, the well-known analytic method of Docobo (1985, 2012) was used. The method is based on a mapping from the interval $(0,2\pi)$ into the set of Keplerian orbits whose corresponding apparent orbits pass through three base points $(\theta_i, \rho_i; t_i)$ $(i = 1, 2, 3)$. In contrast to the Thiele–Innes–van den Bos method, knowledge of the areal constant is not necessary. In a recent paper by Docobo, Tamazian & Campo (2018), the different selection criteria for the orbit were explained: the solution with minimal rms of the O–C residuals from all of the weighted observations, matching dynamical and trigonometric (*Gaia* or *Hipparcos*) parallaxes, and/or the agreement between the calculated masses and those that correspond to the spectral types, etc. The rms error of the residuals is calculated using the following expression:

$$rms = \sqrt{\frac{\sum_{i=1}^{n} w_i (O_i - C_i)^2}{\sum_{i=1}^{n} w_i}}, \quad (1)$$

where $n$ is the number of observations, $O_i$ and $C_i$ are the observed and the calculated values, respectively, and $w_i$ represents the weight assigned for the corresponding $i$ observation.

For each of the orbits generated by this method, the software yields not only the rms (with weights) both for the position angle ($\theta$) and for the angular separation ($\rho$) but also the dynamical parallaxes with the individual masses and the total mass calculated from the *Hipparcos* or *Gaia* parallaxes. We also obtain for each orbit the residuals for $\theta$ and $\rho$ corresponding to the measurements with large weights. With all of these quality controls, the interval of most probable orbits is delimited and the standard errors of each orbital element are deduced.

Dynamical parallaxes and individual masses have been accurately computed using the ANAPAR method, a colour-dependent model comprising an exact analytical theory along with a non-linear mass–luminosity relationship that allows us to take into account the spectral types of the main-sequence components. In addition, their uncertainties have been calculated from uncertainties in the orbital elements and in the apparent magnitudes by means of Monte Carlo simulations. We have compared these dynamical parallaxes with the values provided by *Hipparcos* and *Gaia* DR2. In some cases, the *Gaia* EDR3 provided new values for the parallaxes, and we commented them in the text.

This investigation represents the continuation of the collaboration between the research groups of the Universidad de Chile and the Ramon Maria Aller Astronomical Observatory at the Universidade de Santiago de Compostela for the investigation of binary and multiple stellar systems in the context of the IAU G1 Commission (Gomez et al. 2016; Docobo et al. 2019). A detailed description of the procedure for processing data is described in Tokovinin et al. (2018).

In Section 2, we present the results and discussion with individual comments for each binary. Tables 1–5 summarize the information related to the obtained orbital elements, the ephemerides, the weighted rms quality controls, the masses, and the dynamical parallaxes yielded by previous and new orbits. Figs 1–19 show the apparent orbits along with the available observations. The new orbit is indicated with a solid line and the previous orbit is shown with a broken line. The Fig. 1 caption contains details associated with the plots.

In Section 3, we calculate the absolute magnitudes and luminosities (Table 6) in order to determine the locations of the systems in the HR diagram as plotted relative to the isochrones generated with MESA Isochrones and Stellar Tracks, MIST (Paxton et al. 2011, 2013, 2015; Choi et al. 2016; Dotter 2016). Absolute luminosities for the A 1126, A 2145, and HDS 2570 systems were not included because they have at least one giant component, and for BU 25 because of the existence of a spectroscopic subcomponent for the primary star. The effective temperature was selected from de Jager & Nieuwenhuijzen (1987) according to the spectral type of each component. We used the metallicity data from Ammons et al. (2006), Gontcharov (2012), Gaspar, Rieke & Ballering (2016), and Netopil (2017) to calculate the isochrones when available. Otherwise, we used the metallicity of the Sun. Table 7 shows the data utilized. Figs 20–35 each present one HR diagram per system in which different MIST-generated isochrones are displayed with the position of the system components. Conclusions are discussed in Section 4.

The orbits of the binaries FIN 105, HDS 1091, I 824, HU 874 AB, BU 25, HU 1604, FIN 305, A 1789, HDS 2116 Aa,Ab, A 1126, VOU 44 AB, and HDS 2570 were announced in the IAUDS No 201 (Docobo et al. 2020), and those of the binaries YR 1 Aa,Ab, RST 4155, JC 8, A 2145, RST 3767 AB, BU 350, and A 1141 are published for the first time in this work.

## 2 RESULTS AND DISCUSSION

In Tables 1 and 2, each system is identified in the first column by its Washington Double Star Catalogue (WDS) number (Mason et al. ) and by the discoverer code, which is the name of the binary. In Table 1, we list each binary and the corresponding orbital elements with their standard errors (Columns 2–8): period, $P$, in years; periastron passage, $T$, in years; eccentricity, $e$; the semimajor axis, $a$, in arcseconds; inclination, $i$; angle of the node, $\Omega$, and the argument of the periastron, $\omega$, in degrees. We include the correction for precession used to refer the position angles to the standard equinox of J2000.0 (column 9). The epoch of the last observation used for the orbit calculation is in the same column. Table 2 lists ephemerides for the next 5 yr with $\theta$ values in degrees and those of $\rho$ in arcseconds.

Table 3 contains the magnitudes, the spectral types, the parallaxes, and the calculated masses. In Column 1, the WDS number and the *Hipparcos* identifier (ESA 1997) appear. The name of the binary is in column 2. Columns 3 and 4 list the apparent magnitudes for each component that are preferably taken from the WDS catalogue (Mason et al. 2001). If they do not appear in said catalogue, they are obtained using the SIMBAD total magnitude (Wenger et al. 2000) as well as the magnitude difference given by SOAR speckle observations. The same occurs with the spectral types in Columns 5, 6, and 7. We used the WDS data whenever available. Otherwise, the individual spectral type were obtained from the composite spectrum taking into account the calculated magnitude difference for the system. Columns 8 and 9 show the *Gaia* (Gaia Collaboration 2016, 2018) or the *Hipparcos* (H) parallaxes (Perryman et al. 1997; van Leeuwen 2007) as well

**Table 1.** Orbital elements.

| WDS<br>name | P(yr)<br>$\sigma$ | T(B1950.0)<br>$\sigma$ | e<br>$\sigma$ | a(arcsec)<br>$\sigma$ | i(°)<br>$\sigma$ | Ω(°)<br>$\sigma$ | $\omega$(°)<br>$\sigma$ | Prec. (°)<br>last obs |
|---|---|---|---|---|---|---|---|---|
| 00277-1625 | 6.5343 | 2020.890 | 0.7845 | 0.0674 | 13.17 | 110.27 | 56.98 | 0.0007 |
| YR 1 Aa,Ab | ±0.0210 | ±0.050 | ±0.0110 | ±0.0012 | ±5.0 | ±30.0 | ±30.0 | 2020.8342 |
| 00462-2214 | 49.13 | 2003.96 | 0.261 | 0.162 | 143.8 | 3.1 | 322.5 | 0.0012 |
| RST 4155 | ±0.8 | ±0.25 | ±0.002 | ±0.004 | ±2.0 | ±4.0 | ±5.0 | 2020.9270 |
| 03124-4425 | 45.35 | 2022.65 | 0.872 | 0.407 | 156.1 | 167.8 | 176.1 | 0.0058 |
| JC 8 | ±0.35 | ±0.20 | ±0.015 | ±0.002 | ±10.0 | ±25.0 | ±30.0 | 2020.8344 |
| 07303-5657 | 170.0 | 2046.15 | 0.578 | 0.244 | 153.5 | 52.1 | 107.1 | 0.0095 |
| FIN 105 | ±40.0 | ±10.05 | ±0.17 | ±0.015 | ±3.0 | ±35.0 | ±30.0 | 2018.2355 |
| 07427-3510 | 275.0 | 2017.4 | 0.690 | 0.332 | 115.2 | 93.3 | 200.2 | 0.0062 |
| HDS 1091 | ±50. | ±0.4 | ±0.03 | ±0.026 | ±0.5 | ±1.0 | ±2.0 | 2018.8438 |
| 09110-1929 | 940. | 2029.37 | 0.869 | 0.492 | 130.3 | 116.5 | 18.0 | 0.0040 |
| I 824 | ±140.0 | ±13.23 | ±0.231 | ±0.050 | ±19.7 | ±28.5 | ±40.0 | 2018.2358 |
| 10093 + 2020 | 74.71 | 1991.86 | 0.829 | 0.139 | 160.6 | 127.1 | 91.4 | 0.0028 |
| A 2145 | ±1.2 | ±0.20 | ±0.010 | ±0.002 | ±0.8 | ±20.0 | ±20.0 | 2019.3833 |
| 10116 + 1321 | 17.96 | 2022.828 | 0.930 | 0.117 | 78.5 | 106.2 | 355.2 | 0.0026 |
| HU 874 AB | ±0.35 | ±0.30 | ±0.005 | ±0.001 | ±0.5 | ±2.5 | ±15.0 | 2019.3816 |
| 10217-0946 | 1340. | 1960.53 | 0.297 | 2.546 | 133.9 | 168.2 | 20.3 | 0.0024 |
| BU 25 | ±60.0 | ±2.50 | ±0.025 | ±0.100 | ±1.0 | ±1.0 | ±2.0 | 2018.1811 |
| 11585-2350 | 740.0 | 1950.53 | 0.661 | 0.914 | 44.5 | 137.6 | 14.3 | 0.0000 |
| RST 3767 AB | ±50.0 | ±1.50 | ±0.015 | ±0.035 | ±2.0 | ±4.0 | ±2.0 | 2018.2536 |
| 12111-5302 | 205.0 | 2049.09 | 0.431 | 0.341 | 55.6 | 89.2 | 32.7 | -0.0005 |
| HU 1604 | ±20.0 | ±14.95 | ±0.080 | ±0.003 | ±2.5 | ±3.0 | ±10.0 | 2018.1621 |
| 13117-2633 | 20.07 | 2021.801 | 0.989 | 0.226 | 114.4 | 8.4 | 91.7 | −0.0019 |
| FIN 305[a] | ±0.50 | ±0.80 | ±0.008 | ±0.002 | ±1.0 | ±1.0 | ±3.0 | 2019.0494 |
| 13117-2633 | 40.70 | 2006.5 | 0.045 | 0.219 | 98.6 | 93.3 | 304.5 | -0.0019 |
| FIN 305[b] | ±0.80 | ±1.10 | ±0.025 | ±0.002 | ±1.0 | ±1.0 | ±8.5 | 2019.0494 |
| 13305 + 0729 | 143.44 | 1962.714 | 0.420 | 0.191 | 137.8 | 67.9 | 105.4 | -0.0022 |
| A 1789 | ±1.2 | ±5.0 | ±0.024 | ±0.002 | ±0.5 | ±10.0 | ±5.0 | 2018.2361 |
| 14592-4206 | 58.52 | 2011.10 | 0.304 | 0.287 | 90.9 | 156.1 | 215.1 | -0.0053 |
| HDS 2116 Aa,Ab | ±1.50 | ±0.30 | ±0.009 | ±0.008 | ±0.5 | ±0.5 | ±2.0 | 2019.3798 |
| 15157-2736 | 695.0 | 2020.82 | 0.851 | 0.972 | 138.0 | 178.7 | 188.8 | -0.0048 |
| BU 350 | ±90.0 | ±1.50 | ±0.020 | ±0.035 | ±1.0 | ±1.0 | ±3.5 | 2018.1814 |
| 15493 + 0503 | 289.0 | 1999.09 | 0.647 | 0.197 | 63.5 | 34.4 | 357.9 | -0.0047 |
| A 1126 | ±14.0 | ±0.3 | ±0.015 | ±0.005 | ±0.5 | ±1.0 | ±2.0 | 2019.5387 |
| 16402-2800 | 104.67 | 2067.037 | 0.204 | 0.192 | 41.0 | 13.4 | 154.0 | -0.0060 |
| VOU 44 AB | ±5.0 | ±19.0 | ±0.050 | ±0.015 | ±5.0 | ±8.0 | ±25.0 | 2019.3773 |
| 16458-0046 | 62.39 | 2042.46 | 0.067 | 0.216 | 103.4 | 15.7 | 46.4 | -0.0053 |
| A 1141 | ±0.50 | ±2.50 | ±0.003 | ±0.002 | ±0.5 | ±0.5 | ±11.5 | 2018.1832 |
| 18126 + 1224 | 87.33 | 2010.28 | 0.457 | 0.161 | 73.3 | 131.3 | 153.6 | -0.0057 |
| HDS 2570 | ±0.95 | ±0.40 | ±0.037 | ±0.008 | ±1.0 | ±1.0 | ±1.0 | 2019.5363 |

*Note.*[a]Short orbital solution for FIN 305.
[b]Long orbital solution for FIN 305.

as the total mass deduced using the new orbital parameters. The dynamical parallaxes determined using ANAPAR, appear in Column 10 and the derived individual masses in Columns 11 and 12. All mass values are listed with the associated standard errors. The mass errors were calculated using the propagation of uncertainties. Absolute magnitudes used for calculation were taken from Gray (2005). Both parallaxes are expressed in milliarcseconds (mas) and the masses in solar masses ($M_{\odot}$).

Tables 4 and 5 show the different quality controls used to compare each orbit. First, we calculated the rms error of the differences between the observed and the calculated values of the $\theta$ and $\rho$ coordinates using the data weighting scheme mentioned. We emphasize that the highest weights were assigned to interferometric observations. In Table 5, Column 1 contains the WDS and the *Hipparcos* designations. Column 2 shows the discoverer code (name of the binary). Column 3 presents the author and the year of the previous orbit and Column 4, the *Gaia* or *Hipparcos* parallax value. Columns 5 and 6 show the previous and new values for the dynamical parallaxes, respectively.

### 2.1 WDS 00277-1625 (YR 1 Aa,Ab)

This system has a very short period. Orbits for this system were calculated in 2017 (Cvetković, Pavlović & Boeva 2017) and 2019 (Tokovinin 2019). Both show large rms uncertainties in $\theta$, even though all of the available observations of this system are high

**Table 2.** Ephemerides.

| WDS | Name | 2021.0 | | 2022.0 | | 2023.0 | | 2024.0 | | 2025.0 | |
|---|---|---|---|---|---|---|---|---|---|---|---|
| | | $\theta$ (°) | $\rho$ (arcsec) | $\theta$ (°) | $\rho$ (arcsec) | $\theta$ (°) | $\rho$ (arcsec) | $\theta$ (°) | $\rho$ (arcsec) | $\theta$ (°) | $\rho$ (arcsec) |
| 00277-1625 | YR 1 Aa,Ab | 233.4 | 0.019 | 316.6 | 0.080 | 333.3 | 0.108 | 344.8 | 0.118 | 356.0 | 0.112 |
| 00462-2214 | RST 4155 | 240.2 | 0.164 | 234.7 | 0.169 | 229.7 | 0.175 | 224.9 | 0.180 | 220.4 | 0.184 |
| 03124-4425 | JC 8 | 118.9 | 0.183 | 84.8 | 0.093 | 287.9 | 0.067 | 231.0 | 0.156 | 215.1 | 0.235 |
| 07303-5657 | FIN 105 | 65.7 | 0.233 | 64.0 | 0.228 | 62.2 | 0.223 | 60.3 | 0.218 | 58.3 | 0.212 |
| 07427-3510 | HDS 1091 | 243.1 | 0.076 | 234.6 | 0.069 | 224.4 | 0.064 | 212.7 | 0.060 | 199.9 | 0.058 |
| 09110-1929 | I 824 | 156.8 | 0.074 | 151.3 | 0.073 | 145.7 | 0.072 | 139.9 | 0.071 | 133.9 | 0.070 |
| 10093 + 2020 | A2145 | 223.2 | 0.232 | 222.3 | 0.234 | 221.4 | 0.235 | 220.5 | 0.237 | 219.7 | 0.238 |
| 10116 + 1321 | HU 874 AB | 289.6 | 0.112 | 292.4 | 0.062 | 250.0 | 0.008 | 278.9 | 0.075 | 281.1 | 0.119 |
| 10217-0946 | BU 25 | 127.9 | 1.535 | 127.4 | 1.532 | 126.9 | 1.529 | 126.5 | 1.525 | 126.0 | 1.522 |
| 11585-2350 | RST 3767 AB | 275.7 | 0.590 | 276.3 | 0.597 | 276.9 | 0.605 | 277.5 | 0.612 | 278.1 | 0.619 |
| 12111-5302 | HU 1604 | 37.0 | 0.195 | 36.7 | 0.196 | 42.4 | 0.197 | 45.1 | 0.198 | 47.7 | 0.200 |
| 13117-2633 | FIN 305[a] | 65.7 | 0.064 | 141.9 | 0.029 | 119.5 | 0.076 | 112.6 | 0.105 | 108.5 | 0.127 |
| 13117-2633 | FIN 305[b] | 62.3 | 0.0630 | 36.22 | 0.0401 | 345.77 | 0.0356 | 311.18 | 0.0545 | 296.76 | 0.0811 |
| 13305 + 0729 | A 1789 | 158.5 | 0.196 | 156.9 | 0.197 | 155.3 | 0.197 | 153.7 | 0.198 | 152.2 | 0.199 |
| 14592-4206 | HDS 2116 Aa,Ab | 157.1 | 0.176 | 156.9 | 0.205 | 156.8 | 0.231 | 156.6 | 0.255 | 156.5 | 0.276 |
| 15157-2736 | BU 350 | 350.5 | 0.144 | 341.1 | 0.142 | 331.5 | 0.140 | 321.8 | 0.140 | 312.1 | 0.141 |
| 15493 + 0503 | A 1126 | 143.0 | 0.061 | 147.2 | 0.064 | 151.0 | 0.068 | 154.4 | 0.071 | 157.5 | 0.074 |
| 16402-2800 | VOU 44 AB | 4.8 | 0.227 | 6.7 | 0.227 | 8.5 | 0.227 | 10.3 | 0.227 | 12.1 | 0.226 |
| 16458-0046 | A1141 | 79.6 | 0.058 | 63.6 | 0.068 | 52.5 | 0.082 | 44.7 | 0.098 | 39.0 | 0.113 |
| 18126 + 1224 | HDS 2570 | 348.6 | 0.060 | 357.1 | 0.054 | 7.3 | 0.050 | 19.2 | 0.047 | 32.1 | 0.046 |

*Note*.[a]Short orbital solution for FIN 305.
[b]long orbital solution for FIN 305.

precision speckle observations (ten observations carried out by E. P. Horch from 1977-2014 and four by A. Tokovinin between 2017 and 2020).

Using the new measurement of 2020.8342 obtained with the HRCam@SOAR, we have achieved a solution that yields a rms of 0°.084 in $\theta$ and 0″.0128 in $\rho$, whereas the previous orbit was 18°.719 and 0″.0168 (see Table 4).

Moreover, the dynamical parallax (14.33 ± 0.31 mas) fits the value given by *Gaia* 14.22 ± 0.15 mas (Gaia Collaboration 2018). The inferred masses of the components ($M_A = 1.362 \pm 0.033\ M_\odot$ and $M_B = 1.073 \pm 0.024\ M_\odot$) do not differ much from those that correspond to the F4V + G1V spectral decomposition if we use the table of values of Gray (2005). These spectral types are the result of using the spectral decomposition method proposed by Edwards (1976), taking into account the spectral type of the system (F5/6V) and the difference of magnitude among the components given by SOAR ($\Delta_{m_V} \sim 1.21$). The low inclination (∼ 13°, see Fig. 1) may represent a handicap regarding obtaining a spectroscopic orbit.

### 2.2 WDS 00462-2214 (RST4155)

The orbit presented here represents an improvement of the previous one that was calculated by Heintz (1984). In recent decades, seven more speckle observations were obtained along with that by *Hipparcos* in 1991 (Perryman et al. 1997). The previous orbit had $rms_\theta = 8°.519$ and $rms_\rho = 0''.0287$ while the new orbit decreases them to $rms_\theta = 3°.105$ and $rms_\rho = 0''.0145$. The new dynamical parallax of 9.53 ± 0.30 mas is close to that by *Gaia*, 9.21 ± 0.33 mas (Gaia Collaboration 2018). Using the dynamical parallax, the total mass of the system is $M_T = 2.033\ M_\odot$ with $M_A = 1.043 \pm 0.026\ M_\odot$ and $M_B = 0.990 \pm 0.024\ M_\odot$. These values are in accord with those expected for a system on the basis of the combined spectrum F9V + G1V assigned by using the previously cited algorithm. In Fig. 2, the previous orbit (Heintz 1984) and that contributed in this paper are shown.

### 2.3 WDS 03124-4425 (JC 8)

In 1935, Finsen (1935) calculated an orbital solution for this system for the first time that was followed by those presented by Wierzbiński (1958), Eggen (1965), Starikova (1977a), Heintz (1979), and Söderhjelm (1999). Our solution reduces the rms uncertainty in $\theta$ of the orbit of Söderhjelm (1999), from 4°.733 to 1°.930. In addition, the dynamical parallax associated with the new orbit, 23.58 ± 0.24 mas, approximates the value given by *Hipparcos*, 23.53 ± 0.62 mas. The spectral decomposition of the system given in Simbad is A8V + F3V, while the masses that we obtain for each component are $M_A = 1.365 \pm 0.031\ M_\odot$ and $M_B = 1.134 \pm 0.024\ M_\odot$ which correspond with the ranges of F5V-F8V for the main and F8V-G0V for the secondary according to the values given by Gray (2005). This may be due to an incorrect spectral classification of the star. The A8V + F3V decomposition adopted in Simbad comes from (Malaroda 1973), but there are other listed measurements, some of them assigning a combined spectrum of F6III (de Vaucouleurs 1957; Buscombe & Morris 1958; Edwards 1976), F2 (Cannon & Pickering 1918-1924), and F5V (Houk 1978). This last value appears to be more plausible, considering the calculated mass yielded by our orbit, the absolute magnitudes obtained from

**Table 3.** Magnitudes, spectral types, parallaxes, and masses. The $\Pi^{Sat}$ column contains *Gaia* or *Hipparcos* values of parallaxes, given in miliarcseconds. The H superscript means that the parallax value comes from *Hipparcos*, no superscript indicates *Gaia*. $M_{AB}^{Sat}$ shows the total mass (in units of $M_{\odot}$) derived from these parallaxes with the same superscripts.

| WDS<br>*Hipparcos* | Name | $m_A$ | $m_B$ | $Sp_{AB}$ | $Sp_A$ | $Sp_B$ | $\Pi^{Sat}$<br>$\sigma$ | $M_{AB}^{Sat}$<br>$\sigma$ | $\Pi^{dyn}$<br>$\sigma$ | $M_A^{dyn}$<br>$\sigma$ | $M_B^{dyn}$<br>$\sigma$ |
|---|---|---|---|---|---|---|---|---|---|---|---|
| 00277-1625 | YR 1 Aa,Ab | 7.51 | 8.72 | F5/6V | F4V | G1V | 14.22 | 2.49 | 14.33 | 1.36 | 1.07 |
| | | | | | | | ±0.15 | ±0.16 | ±0.31 | ±0.03 | ±0.02 |
| 00462-2214 | RST 4155 | 9.76 | 10.03 | G0V | F9V | G1V | 9.21 | 2.26 | 9.53 | 1.04 | 0.99 |
| | | | | | | | ±0.33 | ±0.30 | ±0.30 | ±0.03 | ±0.02 |
| 03124-4425 | JC 8 | 6.42 | 7.36 | A8V + F3V | A8V | F3V | $23.53^H$ | $2.52^H$ | 23.58 | 1.37 | 1.13 |
| | | | | | | | ±0.62 | ±0.21 | ±0.24 | ±0.03 | ±0.02 |
| 07303-5657 | FIN 105 | 9.55 | 9.62 | F6V | F6V | F6V | | | 5.7 | 1.35 | 1.33 |
| | | | | | | | | | ±1.5 | ±0.13 | ±0.13 |
| 07427-3510 | HDS 1091 | 10.04 | 10.59 | G1V | G0V | G4V | 4.86 | 4.22 | 6.0 | 1.20 | 1.08 |
| 37578 | | | | | | | ±0.30 | ±1.99 | ±1.1 | ±0.10 | ±0.09 |
| 09110-1929 | I 824 | 9.30 | 9.40 | F0 | F0V | F0V | 3.33 | 3.64 | 3.34 | 1.83 | 1.79 |
| | | | | | | | ±0.20 | ±1.69 | ±0.60 | ±0.16 | ±0.15 |
| 10093 + 2020 | A2145 | 7.30 | 7.50 | G8III + A2m | G8III | A2V | 3.63 | 10.06 | – | – | – |
| 49747 | | | | | | | ±0.56 | ±4.69 | – | – | – |
| 10116 + 1321 | HU 874 AB | 6.90 | 7.87 | F6V | F4V | G0V | $15.48^H$ | $1.34^H$ | 11.75 | 1.68 | 1.38 |
| 49929 | | | | | | | ±0.72 | ±0.20 | ±0.23 | ±0.04 | ±0.03 |
| 10217-0946 | BU 25 | 8.41 | 8.96 | G5 | G3V | G7V | 16.25 | 2.14 | – | – | – |
| 50747 | | | | | | | ±0.10 | ±0.32 | – | – | – |
| 11585-2350 | RST 3767 AB | 10.85 | 11.08 | K0 | K0V | K1V | 9.06 | 1.88 | 9.37 | 0.86 | 0.83 |
| | | | | | | | ± 0.67 | ±0.53 | ± 0.66 | ± 0.03 | ± 0.03 |
| 12111-5302 | HU 1604 | 10.19 | 10.54 | G0 | F9V | G1V | 7.86 | 1.94 | 7.75 | 1.05 | 0.98 |
| 59395 | | | | | | | ±0.80 | ±0.71 | ±0.62 | ±0.04 | ±0.04 |
| 13117-2633 | FIN 305[a] | 7.20 | 7.43 | A5V | A5V | A6V | 7.08 | 80.72 | 23.17 | 1.18 | 1.13 |
| 64375 | | | | | | | ±0.72 | ±25.04 | ±0.56 | ±0.04 | ±0.04 |
| 13117-2633 | FIN 305[b] | 7.20 | 7.43 | A5V | A5V | A6V | 7.08 | 17.87 | 12.89 | 1.52 | 1.44 |
| 64375 | | | | | | | ±0.72 | ±5.52 | ±0.27 | ±0.06 | ±0.05 |
| 13305 + 0729 | A 1789 | 9.14 | 9.39 | A5 | A5V | A6V | $4.83^H$ | $3.01^H$ | 4.79 | 1.58 | 1.50 |
| 65897 | | | | | | | ±0.85 | ±1.59 | ±0.07 | ±0.04 | ±0.04 |
| 14592-4206 | HDS 2116 Aa,Ab | 3.34 | 4.71 | B2V | B2V | B3V | 7.46 | 16.63 | 8.14 | 8.38 | 4.41 |
| 73334 | | | | | | | ±0.70 | ±4.96 | ±0.33 | ±0.27 | ±0.36 |
| 15157-2736 | BU 350 | 7.06 | 8.58 | F2 | F0IV | F6V | $8.19^H$ | $3.46^H$ | 8.26 | 1.98 | 1.39 |
| 74675 | | | | | | | ±0.88 | ±1.48 | ±0.71 | ±0.11 | ±0.01 |
| 15493 + 0503 | A 1126 | 9.40 | 9.40 | K0 | K0III | K0III | 2.62 | 5.09 | – | – | – |
| 77489 | | | | | | | ±0.06 | 0.72 | – | – | – |
| 16402-2800 | VOU 44 AB | 9.19 | 10.61 | F0/2V | A9V | F8V | 6.00 | 2.99 | 6.44 | 1.38 | 1.04 |
| | | | | | | | ±0.43 | ±0.99 | ±0.64 | ±0.09 | ±0.06 |
| 16458-0046 | A1141 | 9.10 | 9.20 | F8 | F7V | F8V | 8.47 | 4.26 | 10.49 | 1.14 | 1.12 |
| 82062 | | | | | | | ±0.48 | ±0.90 | ±0.14 | ±0.03 | ±0.02 |
| 18126 + 1224 | HDS 2570 | 8.04 | 8.88 | F0 | F0III | A6V | 4.71 | 5.237 | – | – | – |
| 89235 | | | | | | | ±0.16 | ±1.481 | – | – | – |

*Note.* [a]Short orbital solution for FIN 305.
[b]Long orbital solution for FIN 305.

the *Hipparcos* parallax (3.28 for the primary and 4.21 for the secondary), and even the colour index, using the values listed in Simbad for the combined $B$ and $V$ magnitudes of the system, $B - V = 0.44$.

### 2.4 WDS 07303-5657 (FIN 105)

The first visual observation of this system occurred in mid-1929 (Finsen 1932). Between 1941 and 1983, a total of seven visual observations were reported from 136° to 106°. The *Hipparcos* reductions resolve the system but do not provide any value for the parallax nor do the measurements of the *Gaia* satellite.

The last available observation used for the calculation of the orbit ($t$= 2018.2355, $\theta$ = 70°03, $\rho = 0''.2465$) was performed at SOAR. This was the first high precision observation obtained for this system, as we can see in Fig. 4.

Due to the similar magnitudes of the components, the composite spectrum, F6V (Houk & Cowley 1975), can be separated into two

**Table 4.** RMS quality controls.

| WDS | Name | New orbit RMS $\Delta\theta$ | New orbit RMS $\Delta\rho$ | Previous orbit RMS $\Delta\theta$ | Previous orbit RMS $\Delta\rho$ |
|---|---|---|---|---|---|
| 00277-1625 | YR 1 Aa,Ab | 0.843 | 0.0128 | 18.719 | 0.0168 |
| 00462-2214 | RST 4155 | 3.105 | 0.0145 | 8.519 | 0.0287 |
| 03124-4425 | JC 8 | 1.930 | 0.0427 | 4.733 | 0.0421 |
| 07303-5657 | FIN 105 | 5.363 | 0.0262 | – | – |
| 07427-3510 | HDS 1091 | 0.414 | 0.0023 | 0.433 | 0.0020 |
| 09110-1929 | I 824 | 2.219 | 0.0369 | – | – |
| 10093 + 2020 | A2145 | 4.775 | 0.0156 | 8.873 | 0.0202 |
| 10116 + 1321 | HU 874 AB | 2.871 | 0.0211 | 8.240 | 0.0474 |
| 10217-0946 | BU 25 | 0.986 | 0.0690 | 1.278 | 0.0664 |
| 11585-2350 | RST 3767 AB | 4.780 | 0.0478 | 6.254 | 0.0600 |
| 12111-5302 | HU 1604 | 3.965 | 0.0397 | – | – |
| 13117-2633 | FIN 305[a] | 5.763 | 0.0168 | 6.339 | 0.0134 |
| 13117-2633 | FIN 305[b] | 5.768 | 0.0270 | 6.339 | 0.0134 |
| 13305 + 0729 | A 1789 | 5.991 | 0.0687 | 9.694 | 0.0593 |
| 14592-4206 | HDS 2116 Aa,Ab | 0.887 | 0.0445 | – | – |
| 15157-2736 | BU 350 | 2.437 | 0.0576 | – | – |
| 15493 + 0503 | A 1126 | 6.967 | 0.0167 | – | – |
| 16402-2800 | VOU 44 AB | 1.054 | 0.0048 | – | – |
| 16458-0046 | A1141 | 5.439 | 0.0193 | 7.376 | 0.0218 |
| 18126 + 1224 | HDS 2570 | 0.981 | 0.0025 | – | – |

*Note.* [a]Short orbital solution for FIN 305.
[b]Long orbital solution for FIN 305.

F6V stars. For our calculations, we determined that the combined $m_V = 8.87$ (Høg et al. 2000) value corresponds to $m_V = 9.55$ for the primary and $m_V = 9.62$ to the secondary. The dynamical parallax obtained from the new orbit (5.7 ± 1.5 mas) yields values of masses, $M_A = 1.35 \pm 0.13\,M_\odot$ and $M_B = 1.33 \pm 0.13\,M_\odot$, that agree with those assigned to F6V spectral types in Gray (2005).

The rms uncertainty in position angle and separation, rms($\theta$, $\rho$) = (5°.363, 0″.0262), are relatively small considering the limited amount of measurements available for the determination of the orbital elements. The orbit should be considered to be preliminary until it is possible to obtain measurements when the separations between the components will be smaller in the near future.

### 2.5 WDS 07427-3510 (HDS 1091)

In this report, we offer an alternative orbit with a considerably greater period, P = 275 yr, as compared to that presented by Tokovinin et al. (2019), P = 120.6 yr, as we can see in Fig. 5. The new orbital elements are quite different from the orbital elements of the previous solution but both yield rms uncertainties that are similar in $\theta$, 0°.414 versus 0°.433, as well as in $\rho$, 0″.0023 versus 0″.0020. The dynamical parallaxes of both orbits are also similar, 5.89 mas for Tokovinin et al. (2019) versus 6.0 ± 1.1 mas, and in agreement with the vales provided by *Gaia* (4.86 ± 0.30 mas in the DR2 and 5.95 ± 0.31 mas in the EDR3). Future observations will permit more accurate determinations of the orbital elements.

### 2.6 WDS 09110-1929 (I 824)

The system I824 presents a variability of the delta Scuti type (Smalley et al. 2011), with a parallax that is estimated by *Gaia* to be 3.33 ± 0.20. The first visual observations were obtained by R. T. A. Innes in the early 1900s (Aitken & Doolittle 1932). In total, there are ten micrometric observations including the last that was conducted by Heintz in 1985. The SOAR observation ($t = 2018.2358, \theta = 170°.63$, $\rho = 0''.0788$) is the second speckle observation that was carried out approximately 30 yr after that by McAllister in 1989.

The weight of these two measurements allows us determine the first orbit for this system with a period of 940 yr and a periastron passage estimated for the end of this decade (see Table 1). The dynamical parallax (3.34 ± 0.60 mas) coincides with that given by *Gaia* DR2 (3.33 ± 0.20 mas), and it is close tothe value of the EDR3 (3.48 ± 0.29 mas). The obtained masses ($M_A = 1.83 \pm 0.16\,M_\odot$ and $M_B = 1.79 \pm 0.15\,M_\odot$) are slightly superior to that expected for type F0V stars.

The rms uncertainty in position angle and separation, 2°.219 and 0″.0369, are relatively small but we cannot consider it to be very relevant because of the small arc covered by the available observations. The good fit between the orbit and both the micrometric and speckle observations can be appreciated in Fig. 6. The imminent periastron passage should be taken advantage of in order to obtain new speckle registers that are fundamental for the tracking of this binary.

### 2.7 WDS 10093 + 2020 (A 2145)

The first orbit for this system was calculated by Baize (1957) and later orbits were determined by Starikova (1977b), Finsen (1977), Tokovinin (1987), Olevic & Cvetkovic (2004), and Mason & Hartkopf (2011). The first orbits gradually increased the value of the period from 60.0 yr (Baize 1957) to 71.1 yr Tokovinin (1987). Olevic & Cvetkovic (2004) calculated an orbit based on visual observations that was much slower with P = 119.25 ± 3.62 yr. The solution of Mason & Hartkopf (2011) and that presented in

**Table 5.** *Gaia* & *Hipparcos* versus dynamical parallaxes. $\Pi^{Sat}$ represents *Gaia* or *Hipparcos* values of parallaxes. The H superscript means *Hipparcos* parallax. No superscript means *Gaia* parallax.

| WDS *Hipparcos* | Name | Previous orbit Author (yr) | $\Pi^{Sat}$ $\sigma$ | Previous orbit $\Pi^{dyn}$ | New orbit $\Pi^{dyn}$ $\sigma$ |
|---|---|---|---|---|---|
| 00277-1625 | YR 1 Aa,Ab | Tokovinin | 14.22 | 16.30 | 14.33 |
| | | (2019) | ±0.15 | – | ±0.31 |
| 00462-2214 | RST 4155 | Heintz | 9.21 | 12.18 | 9.53 |
| | | (1984) | ±0.33 | – | ±0.30 |
| 03124-4425 | JC 8 | Soderhjelm | $23.53^{H}$ | 23.90 | 23.58 |
| | | (1999) | ±0.62 | – | ±0.24 |
| 07303-5657 | FIN 105 | | | | 5.70 |
| | | | | | ±1.50 |
| 07427-3510 | HDS 1091 | Tokovinin et al. | 4.86 | 5.89 | 6.00 |
| 37578 | | (2019) | ±0.30 | – | ±1.10 |
| 09110-1929 | I 824 | | 3.33 | – | 3.34 |
| | | | ±0.20 | – | ±0.60 |
| 10093 + 2020 | A2145 | Mason & Hartkopf | 3.63 | – | – |
| 49747 | | (2011) | ±0.56 | – | – |
| 10116 + 1321 | HU 874 AB | Mason & Hartkopf | $15.48^{H}$ | 14.64 | 11.75 |
| 15.48 49929 | | (2011) | ±0.72 | ±1.01 | ±0.23 |
| 10217-0946 | BU 25 | Tokovinin & Latham | 16.25 | – | – |
| 50747 | | (2020) | ±0.10 | – | – |
| 11585-2350 | RST 3767 AB | Josties & Mason | 9.06 | 63.71 | 9.37 |
| | | (2019) | ± 0.67 | – | ±0.66 |
| 12111-5302 | HU 1604 | | 7.86 | – | 7.75 |
| 59395 | | | ±0.80 | – | ±0.62 |
| 13117-2633 | FIN 305[a] | Tokovinin | 7.08 | 9.72 | 23.17 |
| 64375 | | (2018) | ±0.72 | ±0.45 | ±0.56 |
| 13117-2633 | FIN 305[b] | Tokovinin | 7.08 | 9.72 | 12.89 |
| 64375 | | (2018) | ±0.72 | ±0.45 | ±0.27 |
| 13305 + 0729 | A 1789 | Heintz | $4.83^{H}$ | 4.36 | 4.79 |
| 65897 | | (1998) | ±0.85 | – | ±0.07 |
| 14592-4206 | HDS 2116 Aa,Ab | | 7.46 | – | 8.14 |
| 73334 | | | ±0.70 | – | ±0.33 |
| 15157-2736 | BU 350 | | $8.19^{H}$ | – | 8.26 |
| 74675 | | | ±0.88 | – | ±0.71 |
| 15493 + 0503 | A 1126 | | 2.62 | – | – |
| 77489 | | | ±0.06 | – | – |
| 16402-2800 | VOU 44 AB | | 6.00 | – | 6.44 |
| | | | ±0.43 | – | ±0.64 |
| 16458-0046 | A1141 | Heintz | 8.47 | 8.51 | 10.49 |
| 82062 | | (1982) | ±0.48 | – | ±0.14 |
| 18126 + 1224 | HDS 2570 | | 4.71 | – | – |
| 89235 | | | ±0.16 | – | – |

*Note.* [a]Short and long orbital solution for FIN 305.
[b]Long orbital solution for FIN 305.

this report are based on the most recent high precision observations obtained using speckle interferometry, because of the programs of Calern, SAO, WIYN, and SOAR, and suggest an orbital period that is closer to that given by Tokovinin (1987).

The five new observations at SOAR during the past decade allow the refinement of the orbit of Mason & Hartkopf (2011). Using the new calculation, the period changes from 80.59 to 74.71 yr As a giant component exists within the system (G8III + A2V), the calculation of the dynamical parallax is not reliable and it has not been included in Tables 3 and 5. The new orbit improves the rms yielding a decrease in $\mathrm{rms}_\theta$ from 8°873 to 4°775 and, in $\mathrm{rms}_\rho$, from 0″0202 to 0″0156. The previous and the new orbits are shown in Fig. 7.

### 2.8 WDS 10116 + 1321 (HU 874 AB)

The system HU 874 AB (34 Leo) has a parallax of 15.48 ± 0.72 mas as given by *Hipparcos*. The first visual observation took place in 1905 (W. J. Hussey) and the first speckle observation in 1980 (H.

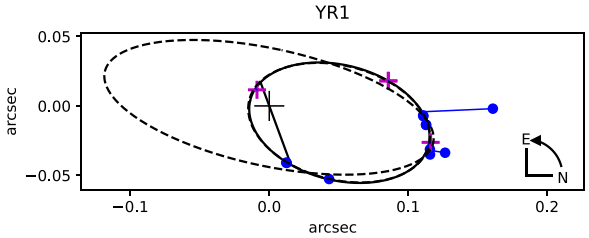


**Figure 1.** For all the Figures and following the Sixth Catalogue of Orbits of Visual Binary Stars (ORB6) standards, the micrometric observations are plotted as the green crosses (+), *Hipparcos* as a red H (H), the interferometric observations are identified by the blue circles, which are filled (•) in the case of speckle interferometry and other high angular resolution techniques, and open (°) for eyepiece interferometry measurements, and the latest ones obtained by SOAR are designated with the magenta crosses (+). All of these symbols are united by their respective colour line to the new orbit, joining the real observation with its expected position according to the time of observation. The previous apparent orbit is represented by a black-dashed line and our new apparent orbit by a solid line. The line of nodes is traced by a solid straight line upon which the position of the primary star can be seen as a large cross. In the right corner, we indicate the orientation of the axes, and the direction of orbital motion. The new orbit of YR 1 Aa,Ab (the shorter period orbit) is compared to the previous one.

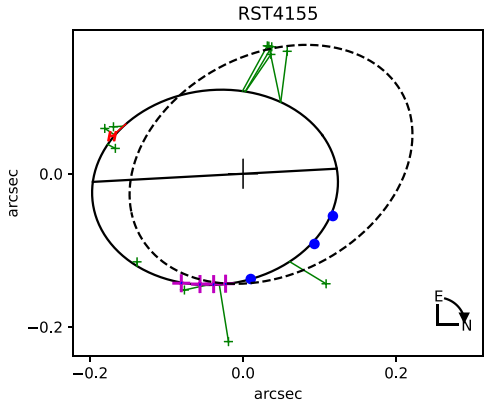


**Figure 2.** RST 4155 orbit fits better the speckle observations.

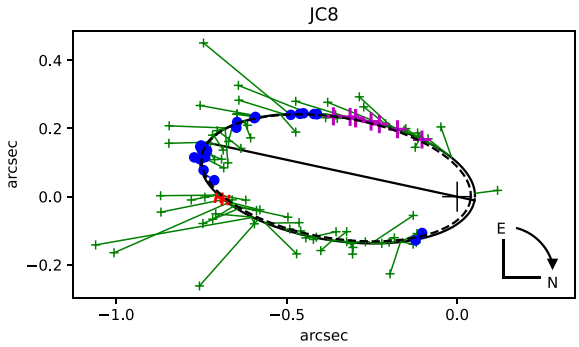


**Figure 3.** JC 8 previous and new apparent orbits.

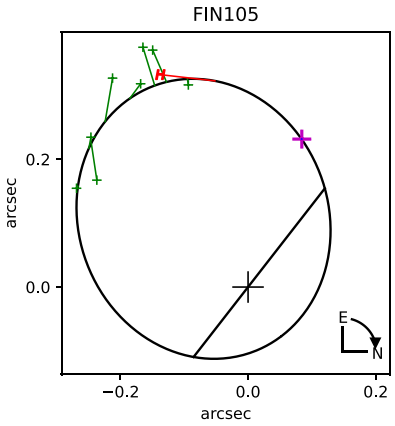


**Figure 4.** FIN 105 first orbit.

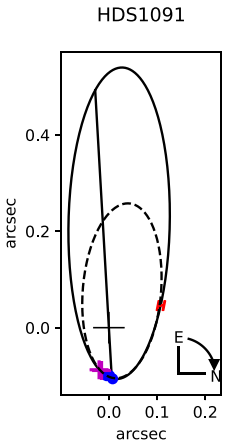


**Figure 5.** The apparent orbit of HDS 1091 orbit compared with the previous one.

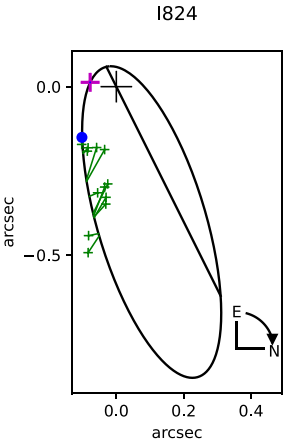


**Figure 6.** I 824 first orbit.

A. McAllister). Of the total of 73 measurements, the last four were obtained using the HRCam@SOAR. The first orbit for this system was calculated by Baize (1984) and was improved because of speckle observations by Hartkopf, Mason & McAlister (1996). Measurements obtained since then allow us to determine a new orbit with a period of 17.962 yr and a periastron passage estimated for 2022.828. The dynamical parallax, 11.75 ± 0.23 mas, is lower than that provided by *Hipparcos* (15.48 ± 0.42 mas).

We should consider that the total mass of the system calculated with the *Hipparcos* parallax, $M_T = 1.338\ M_\odot$, seems to be too

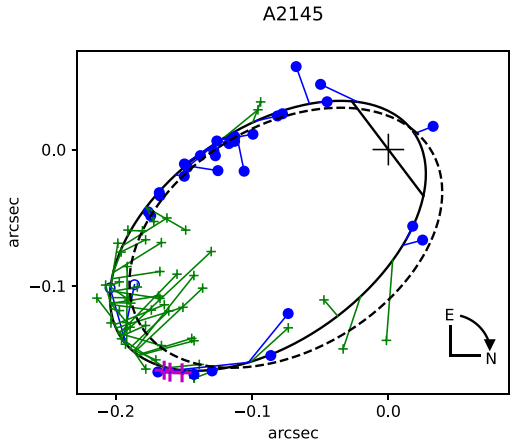


**Figure 7.** A 2145 previous and new apparent orbits.

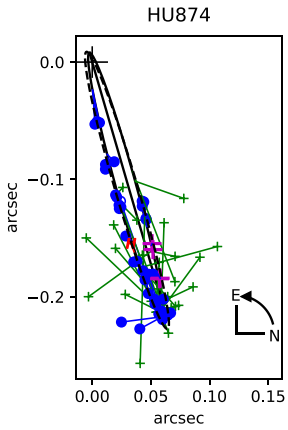


**Figure 8.** New HU 874 orbit compared with previous one.

small for this system. Meanwhile, the total mass obtained with the new dynamical parallax, $M_T = 3.063$ $M_\odot$, breaks down to $M_A = 1.682 \pm 0.042$ $M_\odot$ and $M_B = 1.381 \pm 0.032$ $M_\odot$, both superior to those expected for the type F4V + G0V stars. These spectral types result from applying the previously mentioned spectral decomposition method to the spectral type of the system (F6V) and the difference of magnitude provided by SOAR (∼1.5).

The rms uncertainty in position angle and separation (2°871 and 0″0211, respectively) are smaller than those obtained from the previous orbit calculated by Hartkopf et al. (1996) that shows $rms_\theta = 8°240$ and $rms_\rho = 0''0474$ (see Fig. 8). The eccentricity of the new orbit (0.93) and also the fact that the periastron passage takes place next year are notable features. For that reason, this binary should be a preferred object of observation.

### 2.9 WDS 10217-0946 (BU 25)

The binary BU 25 has a very long period orbit with an *Hipparcos* parallax of 16.68 ± 1.18 mas and a *Gaia* parallax of 16.25 ± 0.10 mas for the DR2, and 15.01 ± 0.08 for the EDR3. The first visual observation was carried out by G. M. Searle in 1867 and the first speckle observation was obtained with the Washington Speckle Interferometer in 1991 (Douglass, Hindsley & Worley 1997). In total, we have 93 available observations of which the last four were conducted using the HRCam@SOAR (see Fig. 9).

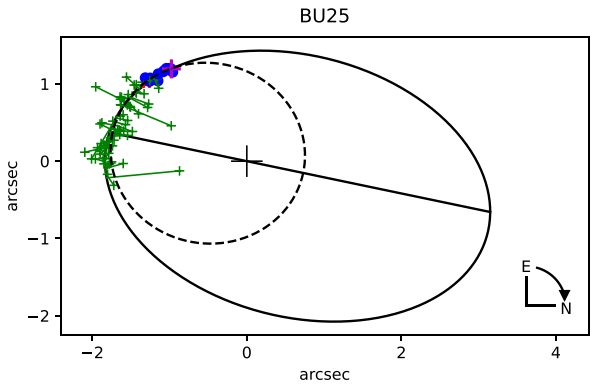


**Figure 9.** BU 25 previous and new apparent orbits.

Due to its slow orbital movement, the first orbit was not calculated until the last decade (Zirm & Rica 2012). In 2019, Izmailov (Izmailov 2019) obtained another solution, and recently, after the calculation of our orbit, an article considering the system as a triple star has been published (Tokovinin & Latham 2020). In this last contribution, the authors present the A component as a SB1, with a orbital period of 8.39 yr and a mass ratio, q = 0.25. Moreover, the postulated masses of the components are: Aa = 1.07 $M_\odot$, Ab = 0.27 $M_\odot$, and B = 0.96 $M_\odot$, which imply, as noted by Tokovinin and Latham, a small but detectable wobble motion in the system. The existence of this spectroscopic subcomponent prevents us from calculating the dynamical parallax of the system, because the ANAPAR algorithm is not calibrated for triple stars.

The corresponding spectral types will be, probably, G3 and M4-5 for the components of the inner binary, and G7 for the B component. Nevertheless, the outer orbit is not currently well defined and the three orbits of Zirm & Rica (circular), Tokovinin & Latham (with small inclination and moderate eccentricity), and that presented herein (with the longest period) remain among the possibilities; they not only yield similar rms uncertainties in theta and rho, but also, when using the *Gaia* parallax, similar inferred total masses.

### 2.10 WDS 11585-2350 (RST 3767 AB)

The new orbit presented here has a long period, i.e. P = 740 yr, and supersedes the orbit ($P = 122.03$ yr) proposed by Josties & Mason (2019).

In addition to improving the rms uncertainty in $\theta$ and in $\rho$, we point out that the dynamical parallax of the new orbit, 9.37 ± 0.66 mas, permits the calculation of a total mass of 1.692 $M_\odot$, with $M_A = 0.864 \pm 0.031$ $M_\odot$ and $M_B = 0.828 \pm 0.030$ $M_\odot$, which approximates that expected for a system that we have resolved as K0V + K1V. The previous orbit does not yield a total mass that is compatible with the component spectral types. Although this system does not have a trigonometric parallax assigned in SIMBAD, the *Gaia* EDR3 lists two objects located at less than 1 arcsec of the coordinates of the system provided by Simbad, with parallaxes of 9.06 ± 0.67 and 8.72 ± 0.71 mas, which are within 1$\sigma$ of the calculated dynamical parallax. Their proper motions and the *G* magnitude also appear to be consistent with the values expected for this binary therefore they are likely to be the components of this system.

As can be seen in Fig. 10, the new orbit fits better with the new high precision speckle measurements obtained by SOAR: ($t$, $\theta$, $\rho$)

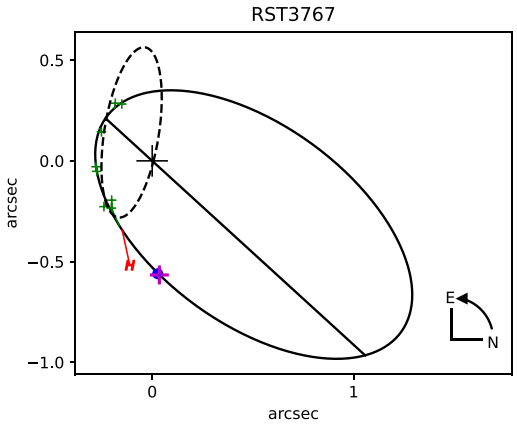


**Figure 10.** RST 3767 AB orbit using the new speckle measurement.

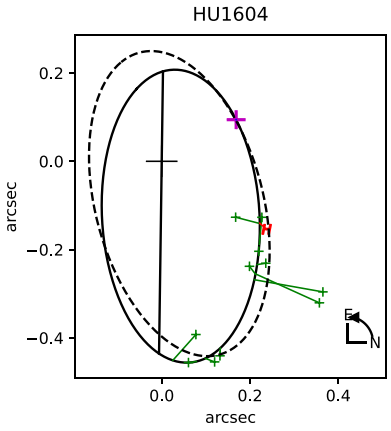


**Figure 11.** First HU 1604 orbit.

= (2016.9603, 272°80, 0″5611) and ($t, \theta, \rho$) = (2018.2536, 273°60, 0″5675).

### 2.11 WDS 12111-5302 (HU 1604)

Although still preliminary, we present the first orbit of this binary using 13 observations performed between 1914 and 2019 of which only the last one measured at SOAR was obtained by speckle interferometry. The resulting solution yields an orbital period of 205 yr.

The corresponding dynamical parallax, 7.75 ± 0.62 mas, is close to the *Gaia* parallax value of 7.86 ± 0.80 mas and both are considerably lower than the value given by *Hipparcos* of 9.66 ± 1.78 mas.

The Simbad data base indicates a G0 spectral type which we have resolved as F9V + G1V. Nevertheless, the calculated masses of $M_A$ = 1.045 ± 0.042 $M_\odot$ and $M_B$ = 0.978 ± 0.039 $M_\odot$ appear to be slightly inferior to those expected for the spectral types. On the other hand, the rms of the orbital residuals, 3°965 in $\theta$ and 0″0397 in $\rho$, are not too large if we keep in mind that there are two micrometric measurements with high O–C differences as shown in Fig. 11.

### 2.12 WDS 13117-2633 (FIN 305)

Previous orbits of this system were calculated by Finsen (1968) and later by Docobo & Andrade (2012, 2013) and Tokovinin (2018c).

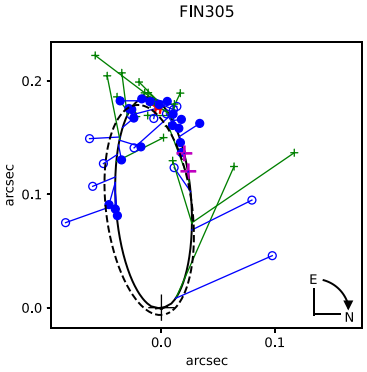


(a) FIN 305 short orbit

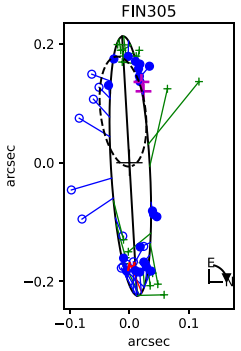


**Figure 12.** FIN 305 short and long orbits.

The short period of the new orbit (Fig. 12a), 20.074 yr, is similar to that of the previous orbit, 19.97 yr, nevertheless, the rms uncertainty in $\theta$ was improved. In addition, we were able to determine a solution with the long period of 40.70 yr by taking advantage of the small difference in magnitude between the components and flipping some position angles. The rms of the residuals for this solution indicates that this orbit is also feasible, especially for the values obtained for the masses. The values of the dynamical parallax (23.17 ± 0.56 mas for the short period orbit, and 12.89 ± 0.87 for the long period solution) differ from that given by *Hipparcos* (7.08 ± 0.72), and the mass sum calculated from this last is unrealistic in both cases, although the masses obtained from the dynamical parallax seem to favour the 40.70 yr solution.

In the different tables, we have written FIN 305$^a$ for the short period orbit and FIN 305$^b$ for the other. See Figs 12(a) and (b).

### 2.13 WDS 13305 + 0729 (A 1789)

The first visual observations of this binary were carried out between 1908 and 1926 by R. G. Aitken. Today there are a total of 29 measurements, five obtained via speckle interferometry, and the last one was measured at SOAR in 2018.2361 (see Fig. 13). Heintz (1998) was the author of the previous orbit. The new solution increases the period from 138 to 143.44 yr and clearly improves the rms uncertainty in $\theta$ (see Table 4). In spite of that, the obtained masses of $M_A$ = 1.581 ± 0.040 $M_\odot$ and $M_B$ = 1.503 (0.036) $M_\odot$ are inferior to those expected for A5V + A6V. However, the dynamical parallax deduced from the new orbit, 4.79 ± 0.07 mas, is in accord with that of *Hipparcos*, 4.83 ± 0.85 mas.

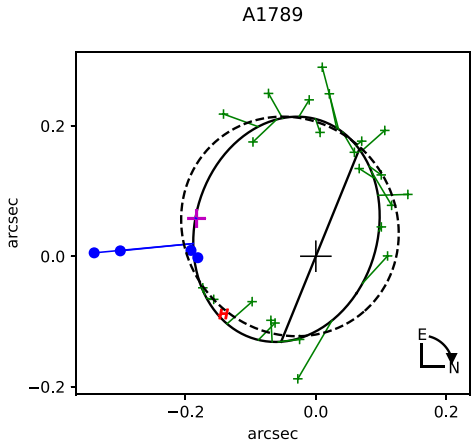


**Figure 13.** The new A 1789 orbit compared with previous orbit.

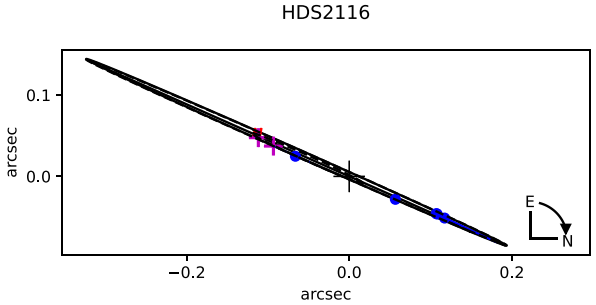


**Figure 14.** HDS 2116 Aa,Ab orbit with a high inclination.

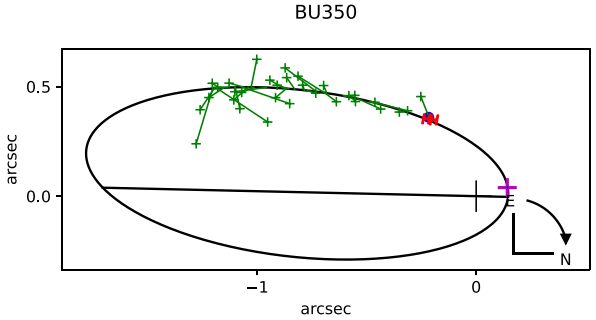


**Figure 15.** BU 350 first orbit.

### 2.14 WDS 14592-4206 (HDS 2116 Aa,Ab)

This binary was not resolved until images contributed by the *Hipparcos* astrometric satellite were reduced (ESA 1997). Previously, this system was only known to contain the AB pair with an angular separation of almost 4 arcsec. It therefore must be a triple system. For the preliminary orbit calculation, we used nine observations of which six were recently carried out by A. Tokovinin. The solution yielded an orbit with a period of of 58.52 yr and an inclination of almost 90° (see Fig. 14).

There is some discrepancy in the literature about the luminosity class corresponding to the combined spectrum of the system. The system has been classified not only as a main-sequence star (Gascoigne 1950; Pagel 1956; Eggen 1961; Buscombe 1962), but also as a subgiant (Hiltner, Garrison & Schild 1969; Houk 1978), or even as a giant (de Vaucouleurs 1957). We considered it as V class (adopting a B2V + B3V decomposition) because on this way a more realistic position of the components on the HR diagram is achieved.

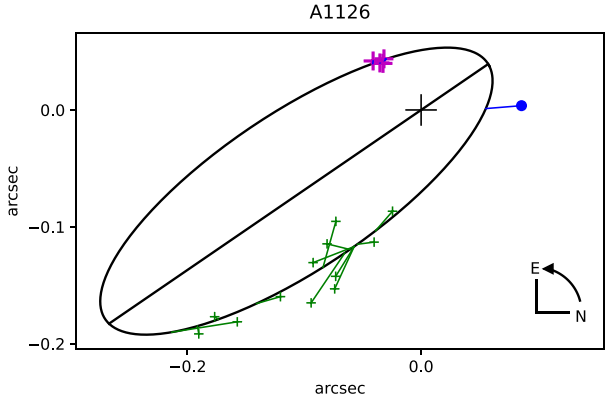


**Figure 16.** A 1126 first orbit.

Nevertheless, it is necessary to take into account that this star was classified as a slowly pulsating B-type star (Rainer et al. 2016).

The dynamical parallax of 8.14 (0.33) mas is very similar to that of *Hipparcos*, 8.51 ± 0.54 mas, and both are slightly higher than the *Gaia* value of 7.46 ± 0.70 mas. With ANAPAR, the following masses were deduced: $M_{Aa} = 8.38 \pm 0.27\ M_\odot$ and $M_{Ab} = 4.41 \pm 0.36\ M_\odot$.

### 2.15 WDS 15157-2736 (BU 350)

We are dealing with a preliminary orbit of a binary with a very long period and high eccentricity. The periastron passage has just occurred and speckle observations are very important at such a time and during the next years in order to define the orbit. It was precisely a SOAR measurement of 2018.1814 that allowed us to obtain this first orbital solution.

The main component is a subgiant and there exists a certain disparity in the values of the parallax. The calculated orbit presents minimal rms, and the dynamical parallax of 8.26 ± 0.71 mas is slightly larger to that of *Hipparcos* of 8.19 ± 0.88 mas. On the other hand, the total mass obtained using the parallax of 3.07 ± 0.81 mas given by *Gaia* seems too high considering that, by using the dynamical parallax, we deduced values that are more in accord with F0IV + F6V, $M_A = 1.98 \pm 0.11\ M_\odot$ and $M_B = 1.39 \pm 0.01\ M_\odot$.

### 2.16 WDS 15493 + 0503 (A 1126)

The SOAR speckle observations between 2017 and 2019 after the periastron passage led to a good definition of the arc around this position. They also offer the possibility to calculate a first orbit with certain guarantees for this system with giant components, K0III + K0III. From now on, the angular separation will increase which will favour its tracking and, therefore, the refinement of its orbit.

Presently, the total mass deduced with the *Gaia* DR2 parallax of 2.62 ± 0.06 mas is 5.0 $M_\odot$. This value is much larger than expected for its spectral types and luminosities. The value of the parallax has been updated in the EDR3 to 2.60 ± 0.04 mas, which yields a mass of 5.2 $M_\odot$.

### 2.17 WDS 16402-2800 (VOU 44 AB)

This is a good example that demonstrates the versatility of the analytic method of orbit calculation of Docobo (1985, 2012). Only with the observations localized in three concrete zones, as shown in Fig. 17, it has been possible to determine a preliminary solution. In this case, we calculated the family of orbits that pass through three points and selected the one that shows a dynamical

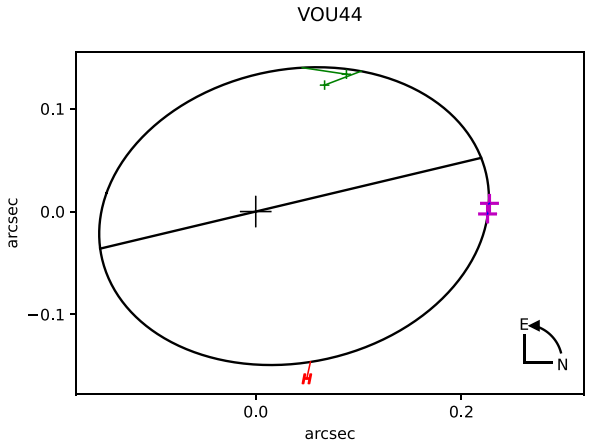


**Figure 17.** VOU 44 first apparent orbit.

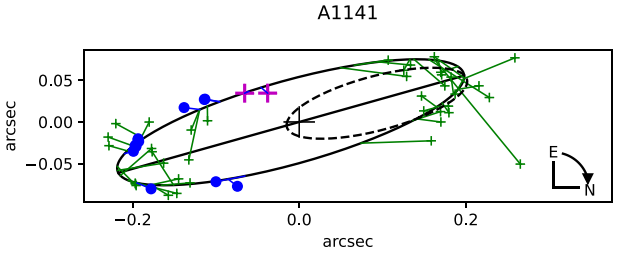


**Figure 18.** A 1141 previous and new apparent orbits.

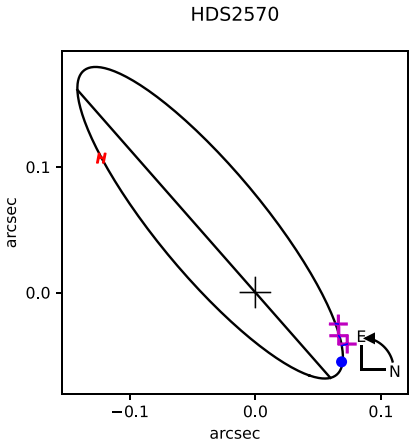


**Figure 19.** HDS 2570 first orbit.

parallax of 6.45 ± 0.65 mas, which is the closest to the parallax of 6.00 ± 0.43 mas given by *Gaia* DR2. In the EDR3 the parallax has been changed to 8.89 ± 0.29, although it is advisable to wait until the full DR3, when the multiplicity of the systems will be considered for the solution.

### 2.18 WDS 16458-0046 (A1141)

Various orbits of this pair have been previously calculated with differences among them, particularly regarding the period. Baize (1976) and Starikova (1981) obtained periods of 62.07 and 64.92 yr. Heintz (1982) flipped the position angle of some measurements by 180° and obtained an orbital period of 30.8 yr, approximately half of each of the two previous values.

**Table 6.** Absolute magnitudes and luminosities obtained from the dynamical parallax.

| Star | $M_{VA}$ | $M_{VB}$ | $L_A$ ($L_\odot$) | $L_B$ ($L_\odot$) |
|---|---|---|---|---|
| YR 1 Aa,Ab | 3.29 | 4.50 | 3.81 ± 0.38 | 1.32 ± 0.13 |
| RST 4155 | 4.66 | 4.93 | 1.15 ± 0.17 | 0.91 ± 0.13 |
| JC 8 | 3.28 | 4.22 | 3.84 ± 0.18 | 1.67 ± 0.08 |
| FIN 105 | 3.33 | 3.40 | 3.69 ± 4.47 | 3.47 ± 4.21 |
| HDS 1091 | 3.93 | 4.48 | 2.16 ± 1.82 | 1.34 ± 1.13 |
| I 824 | 1.92 | 2.02 | 13.22 ± 10.93 | 12.04 ± 9.96 |
| HU 874 AB | 2.25 | 3.22 | 9.74 ± 0.88 | 4.05 ± 0.37 |
| RST 3767 AB | 5.71 | 5.94 | 0.47 ± 0.15 | 0.39 ± 0.13 |
| HU 1604 | 4.64 | 4.99 | 1.17 ± 0.43 | 0.86 ± 0.32 |
| FIN 305[a] | 4.02 | 4.25 | 1.99 ± 0.22 | 1.62 ± 0.18 |
| FIN 305[b] | 2.75 | 2.98 | 6.14 ± 0.59 | 4.99 ± 0.48 |
| A 1789 | 2.54 | 2.79 | 7.44 ± 5.23 | 5.92 ± 4.15 |
| HDS 2116 Aa,Ab | − 2.11 | − 0.74 | 3561.23 ± 664.87 | 491.06 ± 91.68 |
| BU 350 | 1.64 | 3.16 | 17.31 ± 6.85 | 4.25 ± 1.68 |
| VOU 44 AB | 3.23 | 4.65 | 4.00 ± 1.83 | 1.15 ± 0.53 |
| A 1141 | 4.20 | 4.30 | 1.70 ± 0.10 | 1.56 ± 0.10 |

*Note.*[a]Short orbital solution for FIN 305.
[b]Long orbital solution for FIN 305.

Using the solution of Heintz (1982), the dynamical parallax is deduced to be 8.51 mas, which is close to the *Gaia* parallax of 8.47 (0.48) mas and the masses obtained, $M_A = 1.25\,M_\odot$, $M_B = 1.22\,M_\odot$, are in accord with the F7V + F8V spectral types. However, it is possible to obtain a better fit of the orbit to the latest speckle observations, mainly in $\theta$. We have obtained a new orbit that improves the rms uncertainty in $\theta$ and maintains the rms uncertainty in $\rho$. The period of the newly calculated orbit is 62.39 yr. Masses of the components are deduced to be in the G0-G2 spectral type range: $M_A = 1.138 \pm 0.025\,M_\odot$ and $M_B = 1.116 \pm 0.024\,M_\odot$. The dynamical parallax of this new orbit (10.49 ± 0.14 mas) is less in agreement with the value provided by *Gaia* in the DR2, but it is closer to the solution given by *Hipparcos* (9.35 ± 1.13 mas). The value has been revised for the *Gaia* EDR3 to 11.65 ± 0.70 mas.

### 2.19 WDS 18126 + 1224 (HDS 2570)

Four observations have been obtained at SOAR since 2015 that cover the zone of minimum angular separation. Those measurements, along with one given by *Hipparcos*, have allowed us to determine the first orbit of this system. The combined spectral type, along with the absolute magnitude estimated from the trigonometric parallax, suggest the possibility of a giant component within the system. Using the magnitude difference, we adopt a decomposition of F0III + A6V.

A sixth measurement by the Washington Speckle Interferometer in 2002.6260 exists but, according to the authors, it is not certain. Therefore, it was not included in the calculation.

Using the *Hipparcos* parallax of 4.42 ± 0.95 mas, a total mass of $6.38\,M_\odot$ was obtained, dropping to $5.24\,M_\odot$ if the value of the *Gaia* DR2 parallax, 4.71 ± 0.16 mas, is used, and to $3.78\,M_\odot$ with the solution of the *Gaia* EDR3, 5.25 ± 0.14 mas. The last value of the mass may be compatible with proposed spectral types. As this system may contain a giant component, we have not obtained its dynamical parallax so it is not present in Table 3 nor in Table 5.

## 3 LUMINOSITIES AND AGES

The absolute magnitudes of the components were previously obtained, using the dynamical parallaxes, to calculate the luminosities

**Table 7.** Temperature and metallicity.

| WDS *Hipparcos* | Name | Metalicity | Catalogue (yr) | $\log(T_{\rm eff})$ | $v/v_{\rm crit}$ |
|---|---|---|---|---|---|
| 00277-1625 | YR 1 Aa,Ab | −0.19 | Gaspar + (2016) | 3.832 3.768 | 0 |
| 00462-2214 | RST 4155 | 0.01 | Ammons + (2006) | 3.796 3.768 | 0 |
| 03124-4425 | JC 8 | −0.06 | Netopil + (2017) | 3.881 3.840 | 0 |
| 07303-5657 | FIN 105 | −0.04 | Ammons + (2006) | 3.815 3.815 | 0 |
| 07427-3510 37578 | HDS 1091 | 0.02 | Ammons + (2006) | 3.774 3.751 | 0 |
| 09110-1929 | I 824 | 0.29 | Ammons + (2006) | 3.864 3.864 | 0.4 |
| 10116 + 1321 49929 | HU 874 AB | 0.04 | Gaspar + (2016) | 3.832 3.774 | 0 |
| 11585-2350 | RST 3767 AB | 0.0 | Ammons + (2006) | 3.712 3.698 | 0 |
| 12111-5302 59395 | HU 1604 | −0.17 | Ammons + (2006) | 3.796 3.779 | 0 |
| 13117-2633 64375 | FIN 305[a] | 0 | | 3.913 3.901 | 0 |
| 13117-2633 64375 | FIN 305[b] | 0 | | 3.913 3.901 | 0 |
| 13305 + 0729 65897 | A 1789 | 0 | | 3.913 3.901 | 0 |
| 14592-4206 73334 | HDS 2116 Aa,Ab | 0.01 | Gontcharov + (2016) | 4.320 4.274 | 0.4 |
| 15157-2736 74675 | BU 350 | −0.15 | Ammons + (2006) | 3.875 3.815 | 0.4 |
| 16402-2800 | VOU 44 AB | −0.23 | Ammons + (2006) | 3.881 3.796 | 0 |
| 16458-0046 82062 | A1141 | −0.23 | Ammons + (2006) | 3.815 3.796 | 0 |

*Note.* [a]Short orbital solution for FIN 305 are marked with an asterisk, or double asterisk, respectively.
[b]Long orbital solution for FIN 305.

with the expression (Torres 2010):

$$\log\frac{L}{L_{\odot}} = -0.4(M_V - V_{\odot} - 31.572 + (BC_V - BC_{\odot})). \quad (2)$$

As ususal, the symbols, $L$ and $M_V$, represent the luminosity and the absolute $V$ magnitude of the star, $L_{\odot}$ and $V_{\odot}$ are the luminosity and the apparent visual magnitude of the Sun, and $BC_V$ and $BC_{\odot}$ are the bolometric corrections of the star and the Sun in the $V$ band, respectively. We adopted the value of $V_{\odot}$ from Torres (2010) and the bolometric corrections from Straizys & Kuriliene (1981). Table 6 shows the name of the star in the first column. The absolute magnitudes of the components appear in the second and third columns and the luminosities are shown in the fourth and fifth columns.

This methodology was not applied for A 2145, A 1126, and HDS 2570 because ANAPAR is not calibrated for Class III (giants), and for BU 25 due to the presence of an spectroscopic subcomponent therefore those systems do not appear in Table 6 or 7.

To obtain information associated with system ages, we used their metallicity values from Ammons et al. (2006), Gontcharov (2012),

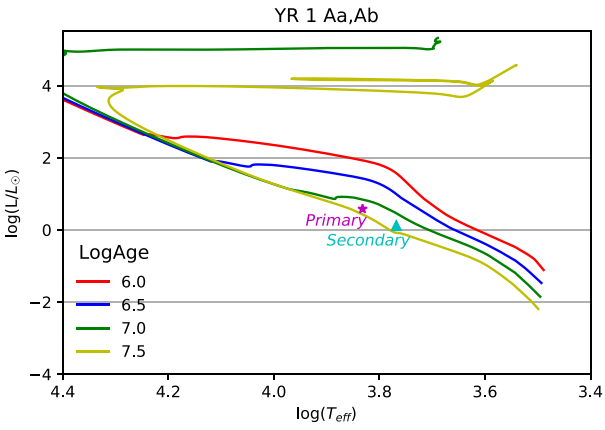


**Figure 20.** YR 1 HR diagram.

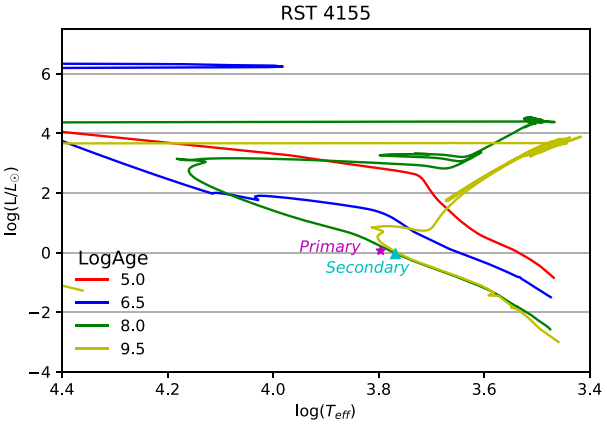


**Figure 21.** RST 4155 HR diagram.

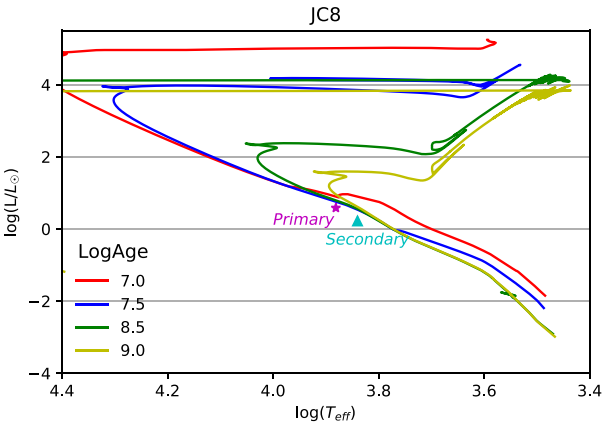


**Figure 22.** JC 8 HR diagram.

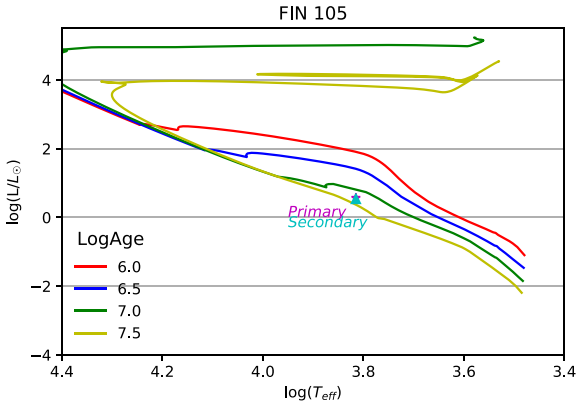


**Figure 23.** FIN 105 HR diagram.

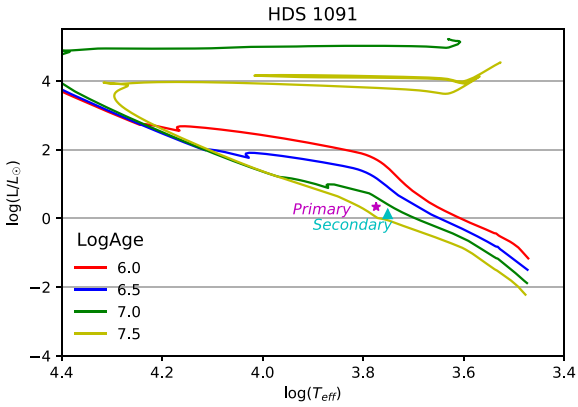


**Figure 24.** HDS 1091 HR diagram.

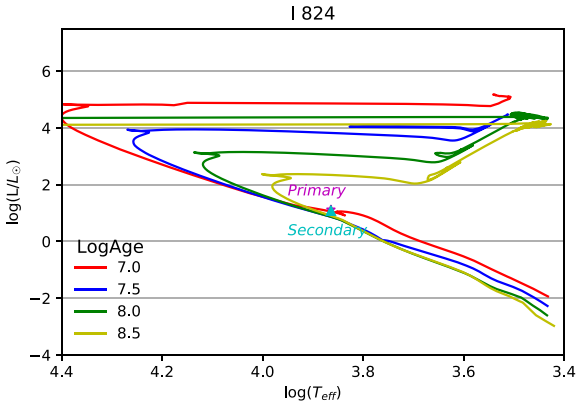


**Figure 25.** I 824 HR diagram.

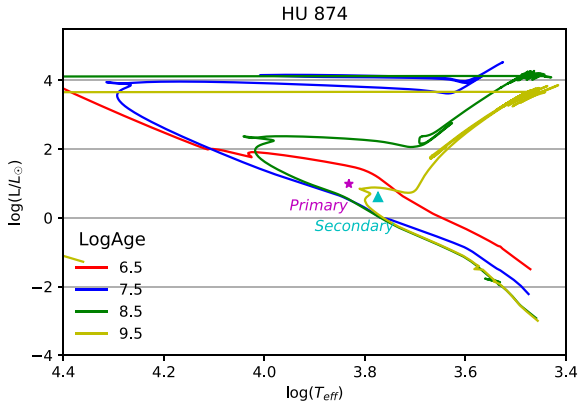


**Figure 26.** HU 874 HR diagram.

Gaspar et al. (2016), and Netopil (2017). We applied the relations between the spectral type and effective temperature given by de Jager & Nieuwenhuijzen (1987). The values utilized to calculate the isochrones can be seen in Table 7. The isochrones were provided by MIST (Paxton et al. 2011, 2013, 2015; Choi et al. 2016; Dotter 2016). MIST uses the value of $v/v_{\rm crit}$ to model the rotation of the star, where $v$ represents the surface linear velocity of the star and $v_{\rm crit}$ is a critical value which indicates a significant mass-loss due to the rotation. For low-mass stars, the model does not consider rotation ($v/v_{\rm crit} = 0$). We set $v/v_{\rm crit} = 0.4$ for I 824, HDS2116 Aa,Ab, and BU 350, and $v/v_{\rm crit} = 0$ for all the remaining systems. We plotted the components of the systems in HR diagrams (see Figs 20–35), also showing the isochrones of the most probable ages of the system. In the case of FIN 305, we found that the luminosities derived from the dynamical parallax of the long orbit are more accurate than those obtained from the short orbit as they fit better with the temperatures associated to the spectral decomposition (see Figs 29–30).

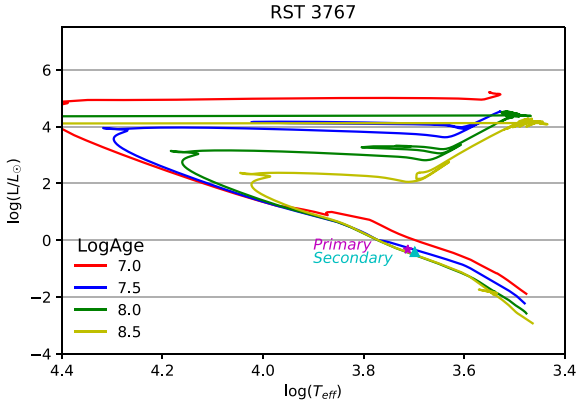


**Figure 27.** RST 3767 AB HR diagram.

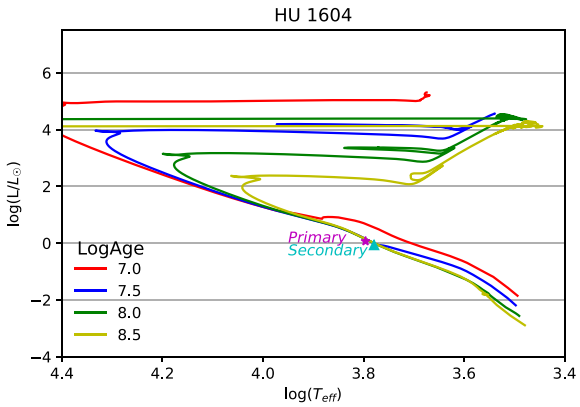


**Figure 28.** HU 1604 HR diagram.

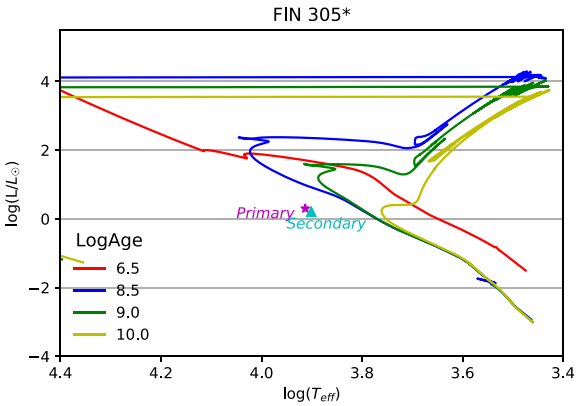


**Figure 29.** FIN 305∗ HR diagram.

Fig. 32 shows that the luminosity value of the secondary component of HDS 2116 Aa,Ab should be higher. The pulsating nature of at least one of the components of the system could be a possible explanation of this discrepancy.

The data do not support a definitive value for some system ages. However, we can see that the calculated luminosities are consistent with system coevolution indicating that both components have the same origin.

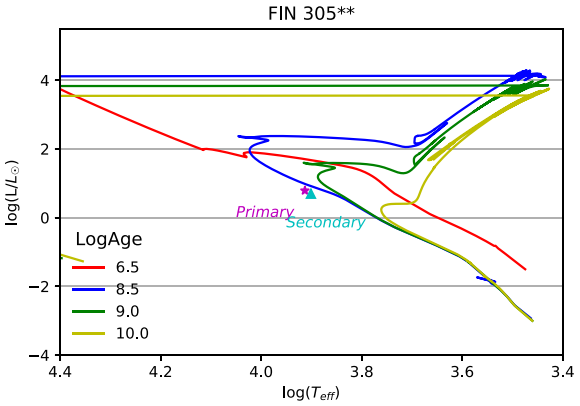


**Figure 30.** FIN 305∗∗ HR diagram.

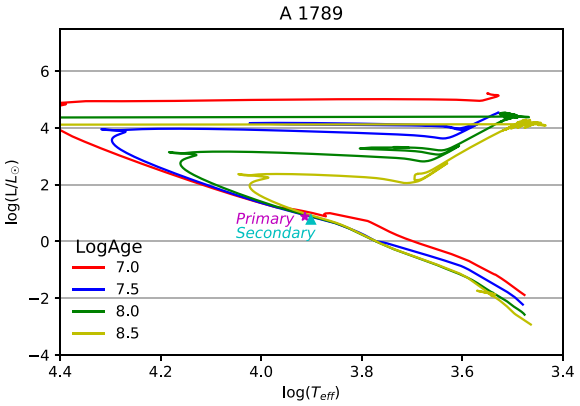


**Figure 31.** A 1789 HR diagram.

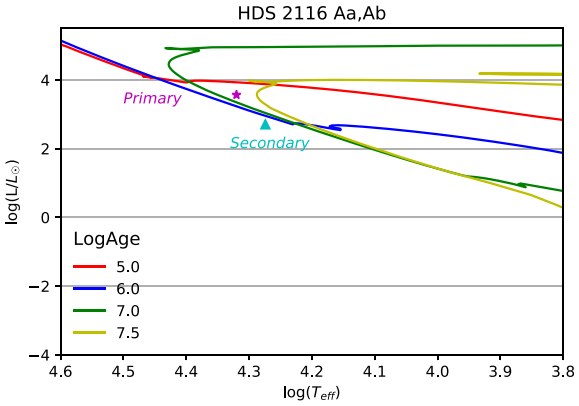


**Figure 32.** HDS 2116 Aa,Ab HR diagram.

Except for HDS 2116 Aa,Ab, the new orbits calculated show a good fit between the luminosities and the spectra assigned to each component according to the decomposition algorithm employed (see Figs 23, 25, 28, 33, and 34).

## 4 CONCLUSIONS

This is the third paper on binaries produced by the collaboration between the Universidad de Chile and the Ramon María Aller Astronomical Observatory that began in 2015. Using SOAR speckle

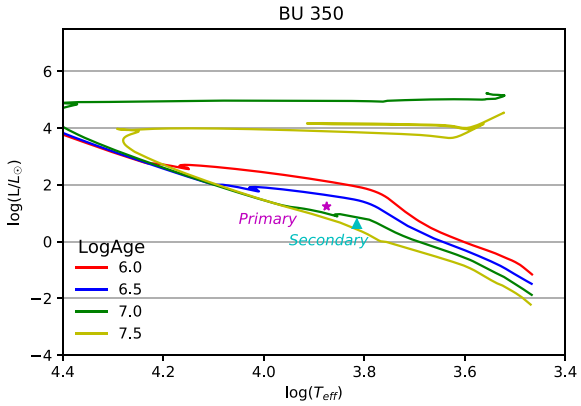


**Figure 33.** BU 350 HR diagram.

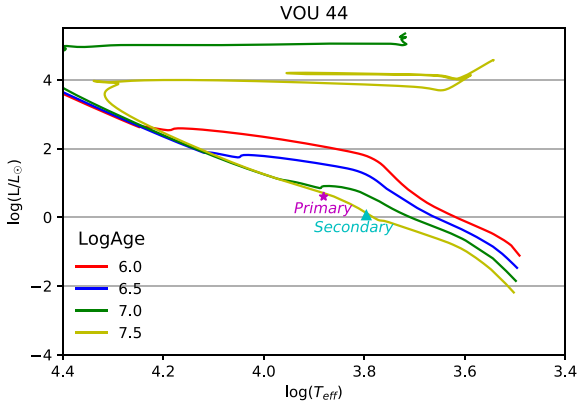


**Figure 34.** VOU 44 HR diagram.

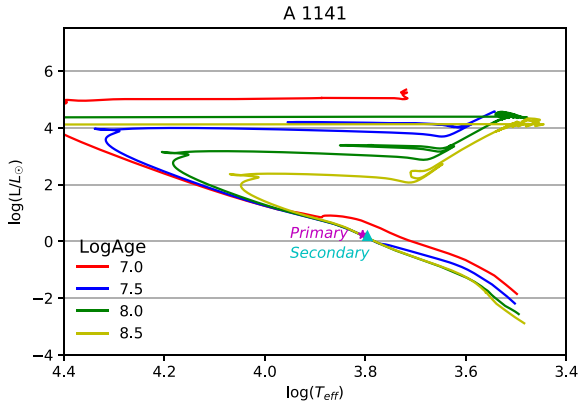


**Figure 35.** A 1141 HR diagram.

measurements collected between 2018 and 2020, we were able to calculate for the first time the orbits of 8 systems and to improve the orbits of 11 more. In one case, FIN 305, we presented two solutions that fit with the observational data available. We also calculated precise dynamical parallaxes for 15 of the systems using the new methodology ANAPAR. Those dynamical parallaxes allowed us to determine the masses and the absolute luminosities for the components of those 15 systems. We used this information together with public data regarding metallicities and effective temperatures to plot their position in the HR diagram against the most suitable isochrones produced by MIST. All of those plots show similar ages for the components and are coherent with a coevolution and common origin context. In the case of HDS 2116 Aa,Ab, the plot shows discrepancies between the luminosities calculated and the effective temperatures expected according to the spectra assigned to each component. Those discrepancies suggest that the dynamical parallaxes must be improved.

The large list of speckle measurements performed by A. Tokovinin, and the quality of them, using the HRCam attached to the 4.1 m. SOAR telescope, confirms the suitability of this instrumentation + telescope in order to continue in the future with this class of observations in benefit of the knowledge of austral close binaries.

## ACKNOWLEDGEMENTS

The authors thank Andrei Tokovinin for his collaboration with speckle runs carried out at SOAR in 2018, 2019, and 2020.

We must also express our deep gratitude to the operator and engineer teams of SOAR that were involved with the observation campaigns.

We are very grateful for the continuous support of the Chilean Telescope Allocation Committee: http://www.das.uchile.cl/das_cntac.html under programs CN2018A-1, CN2019A-2, CN2019B-13, and CN2020A-19 and 2020B-10.

This paper was supported by the 'Xunta de Galicia' (Spain), under the ED431B 2020/38 grant.

RAM and EC acknowledge support from ANID/FONDECYT grant 1190038.

This work used the SIMBAD service operated by the Centre des Données Stellaires (Strasbourg, France, Wenger et al. 2000); bibliographic references from the Astrophysics Data System maintained by SAO/NASA; the Site Informatique des étoiles Doubles de Nice (SIDONIe, Le Contel, Valtier & Bonneau 2001) compiled principally by Dr. Paul Couteau; the historical data base of micrometric measurements provided by the WDS (Mason et al. 2001) the Catalogue of Interferometric Measurements of Binary Stars (WDS INT4, Hartkopf et al. 2001b) and the Sixth Catalogue of Orbits of Visual Binary Stars (WDS ORB6, Hartkopf, Mason & Worley 2001a), all of them maintained at USNO.

This work has used data from the European Space Agency (ESA) mission *Gaia* (https://www.cosmos.esa.int/gaia), processed by the *Gaia* Data Processing and Analysis Consortium (DPAC, https://www.cosmos.esa.int/web/gaia/dpac/consortium). Funding for the DPAC has been provided by national institutions, in particular, the institutions participating in the *Gaia* Multilateral Agreement.

Based on observations obtained at the Southern Astrophysical Research (SOAR) telescope, which is a joint project of the Ministério da Ciência, Tecnologia, e Inovação (MCTI) da República Federativa do Brasil, the U.S. National Optical Astronomy Observatory (NOAO), the University of North Carolina at Chapel Hill (UNC), and Michigan State University (MSU).

## DATA AVAILABILITY

The new measurements used for the calculation will be published in an upcoming article and can be accessed through the Arxiv repository (Tokovinin et al. 2021). The rest of the measurements and the stellar data were obtained from the catalogs and data bases mentioned in the acknowledgements.

## REFERENCES


Aitken R. G., Doolittle E., 1932, New General Catalogue of Double Stars within 120° of the North Pole.Carnegie institution of Washington,Washington
Ammons S. M., Robinson S. E., Strader J., Laughlin G., Fischer D., Wolf A., 2006, ApJ, 638, 1004
Andrade M., 2019, A&A, 630, A96
Baize P., 1957, J. Obs., 40, 17
Baize P., 1976, A&AS, 26, 177
Baize P., 1984, Circ. d'Inf., 94, 1
Buscombe W., 1962, Mount Stromlo Obs. Mimeo., 4, 1
Buscombe W., Morris P. M., 1958, MNRAS, 118, 609
Cannon A. J., Pickering E. C., 1918-1924, Ann. Astron. Obs., 91
Choi J., Dotter A., Conroy C., Cantiello M., Paxton B., Johnson B. D., 2016, ApJ, 823, 102
Cvetković Z., Pavlović R., Boeva S., 2017, AJ, 153, 195
de Jager C., Nieuwenhuijzen H., 1987, A&A, 177, 217
de Vaucouleurs A., 1957, MNRAS, 117, 449
Docobo J. A., 1985, Celest. Mech., 36, 143
Docobo J. A., 2012, in Arenou F., Hestroffer D., eds, Orbital Couples: Pas de Deux in the Solar System and the Milky Way, Paris Observatory, Paris, France, p. 119
Docobo J. A., Andrade M., 2012, IAU Comm. 26 Inform. Circular (IAUDS), 177, 2
Docobo J. A., Andrade M., 2013, MNRAS, 428, 321
Docobo J. A., Gomez J., Campo P. P., Andrade M., Horch E. P., Costa E., Mendez R. A., 2019, MNRAS, 482, 4096
Docobo J. A., Ling J. F., 2003, A&A, 409, 989
Docobo J. A., Méndez R. A., Campo P. P., Costa E., Gómez J., 2020, IAU Comm. G1 Inform. Circular (IAUDS), 201, 1
Docobo J. A., Tamazian V. S., Campo P. P., 2018, MNRAS, 476, 2792
Dotter A., 2016, ApJS, 222, 8
Douglass G. G., Hindsley R. B., Worley C. E., 1997, ApJS, 111, 289
Edwards T. W., 1976, AJ, 81, 245
Eggen O. J., 1961, R. Greenwich Obs. Bull., 41, 245
Eggen O. J., 1965, AJ, 70, 19
ESA ed., 1997, The HIPPARCOS and TYCHO catalogues. Astrometric and photometric star catalogues derived from the ESA HIPPARCOS Space Astrometry Mission ESA Special Publication Vol. 1200, European Space Agency (ESA)
Finsen W. S. , 1968, Circ. Republic Obs. Johannesburg, 127, 171
Finsen W. S., 1932, Circ. Union Obs. Johannesburg, 86, 237
Finsen W. S., 1935, Circ. Union Obs. Johannesburg, 94, 147
Finsen W. S., 1977, Circ. d'Inf., 71
Gaia Collaboration, 2016, A&A, 595, A2
Gaia Collaboration, 2018, A&A, 616, A1
Gascoigne S. C. B., 1950, MNRAS, 110, 15
Gaspar A., Rieke G. H., Ballering N., 2016, ApJ, 826, 171
Gomez J., Docobo J. A., Campo P. P., Mendez R. A., 2016, AJ, 152, 216
Gontcharov G. A., 2012, Astron. Lett., 38, 771
Gray D. F., 2005, The Observation and Analysis of Stellar Photospheres.Cambridge Univ. Press,Cambridge
Hartkopf W. I., Mason B. D., McAlister H. A., 1996, AJ, 111, 370
Hartkopf W. I., Mason B. D., Worley C. E., 2001a, AJ, 122, 3472
Hartkopf W. I., McAlister H. A., Mason B. D., 2001b, AJ, 122, 3480
Heintz W. D., 1979, PASP, 91, 356
Heintz W. D., 1982, A&AS, 47, 569
Heintz W. D., 1984, AJ, 89, 1063
Heintz W. D., 1998, ApJS, 117, 587
Hiltner W. A., Garrison R. F., Schild R. E., 1969, ApJ, 157, 313
Høg E. et al., 2000, A&A, 355, L27
Houk N., 1978, Michigan Catalogue of Two-Dimensional Spectral Types for the HD Stars.Department. of Astronomy, University of Michigan,Ann Arbor
Houk N., Cowley A. P., 1975, University of Michigan Catalogue of Two-Dimensional Spectral Types for the HD Stars.Department of Astronomy, University of Michigan,Ann Arbor
Izmailov I. S., 2019, Astron. Lett., 45, 30
Josties J., Mason B. D., 2019, IAU Comm. G1 Inform. Circular (IAUDS), 199, 2
Labeyrie A., 1970, A&A, 6, 85
Le Contel D., Valtier J. C., Bonneau D., 2001, A&A, 377, 496
Malaroda S., 1973, PASP, 85, 328
Mason B. D., Hartkopf W. I., 2011, IAU Comm. 26 Inform. Circular (IAUDS), 175, 2
Mason B. D., Hartkopf W. I., Miles K. N., Subasavage J. P., Raghavan D., Henry T. J., 2018, AJ, 155, 215
Mason B. D., Wycoff G. L., Hartkopf W. I., Douglass G. G., Worley C. E., 2001, AJ, 122, 3466
Mendez R. A., Claveria R. M., Orchard M. E., Silva J. F., 2017, AJ, 154, 187
Netopil M., 2017, MNRAS, 469, 3042
Olevic D., Cvetkovic Z., 2004, Serbian Astron. J., 168, 25
Pagel B. E. J., 1956, MNRAS, 116, 10
Paxton B. et al., 2013, ApJS, 208, 4
Paxton B. et al., 2015, ApJS, 220, 15
Paxton B., Bildsten L., Dotter A., Herwig F., Lesaffre P., Timmes F., 2011, ApJS, 192, 3
Perryman M. A. C. et al., 1997, A&A, 323, L49
Rainer M. et al., 2016, AJ, 152, 207
Smalley B. et al., 2011, A&A, 535, A3
Söderhjelm S., 1999, A&A, 341, 121
Starikova G. A., 1977a, Soobchen. Gos. Astr. Inst. Sternberg, 199, 12
Starikova G. A., 1977b, Astron. Tsirkulyar, 961, 7
Starikova G. A., 1981, Sov. Astron. Lett., 7, 130
Straizys V., Kuriliene G., 1981, Ap&SS, 80, 353
Tokovinin A. A., 1987, Sov. Astron. Lett., 13, 448
Tokovinin A., 2016, AJ, 152, 138
Tokovinin A., 2017, AJ, 154, 110
Tokovinin A., 2018a, PASP, 130, 035002
Tokovinin A., 2018b, AJ, 155, 160
Tokovinin A., 2018c, IAU Comm. G1 Inform. Circular (IAUDS), 196, 2
Tokovinin A., 2019, IAU Comm. G1 Inform. Circular (IAUDS), 199, 1
Tokovinin A., Cantarutti R., Tighe R., Schurter P., Martinez M., Thomas S., van der Bliek N., 2016, PASP, 128, 125003
Tokovinin A., Latham D. W., 2020, AJ, 160, 251
Tokovinin A., Mason B. D., Hartkopf W. I., Mendez R. A., Horch E. P., 2015, AJ, 150, 50
Tokovinin A., Mason B. D., Hartkopf W. I., Mendez R. A., Horch E. P., 2018, AJ, 155, 235
Tokovinin A., Mason B. D., Mendez R. A., Costa E., Mann A. W., Henry T. J., 2021, AJ, 162, 41
Tokovinin A., Mason B. D., Mendez R. A., Horch E. P., Briceño C., 2019, AJ, 158, 48
Torres G., 2010, AJ, 140, 1158
van Leeuwen F., 2007, A&A, 474, 653
Wenger M. et al., 2000, A&AS, 143, 9
Wierzbiński S., 1958, Acta Astron., 8, 91
Worley C. E., Douglass G. G., 1997, A&AS, 125, 523
Zirm H., Rica F., 2012, IAU Comm. 26 Inform. Circular (IAUDS), 177, 2


This paper has been typeset from a TEX/LATEX file prepared by the author.